

OSU-HEP-06-5
TUM-HEP-644/06

Discretized Gravity in 6D Warped Space

Florian Bauer^{a†}, Tomas Häggren^{b‡}, and Gerhart Seidl^{c§}

^a*Physik-Department, Technische Universität München
James-Franck-Strasse, D-85748 Garching, Germany*

^b*Department of Theoretical Physics, School of Engineering Sciences
Royal Institute of Technology (KTH) – AlbaNova University Center
Roslagstullsbacken 11, 106 91 Stockholm, Sweden*

^c*Department of Physics, Oklahoma State University
Stillwater, OK 74078, USA*

Abstract

We consider discretized gravity in six dimensions, where the two extra dimensions have been compactified on a hyperbolic disk of constant curvature. We analyze different realizations of lattice gravity on the hyperbolic disk at the level of an effective field theory for massive gravitons. It is shown that a nonzero curvature or warping in radial direction allows to obtain a strong coupling scale, that becomes in the infrared regime larger than in discretized warped five-dimensional space. In particular, when approaching the boundary of the discretized warped hyperbolic disk, the local strong coupling scale in the UV can be as large as the local Planck scale. As an application, we also discuss the generation of naturally small Dirac neutrino masses via a discrete volume suppression mechanism.

†E-mail: fbauer@ph.tum.de

‡E-mail: tomashal@kth.se

§E-mail: gerhart.seidl@okstate.edu

1 Introduction

Theories with gravity in a curved space-time background exhibit a number of intriguing features. The warped metric of the Randall-Sundrum (RS) models [1, 2], for example, allows to address the gauge hierarchy problem¹ by considering our four-dimensional (4D) world as a sub-manifold of a five-dimensional (5D) anti de Sitter space. Apart from that, the AdS/CFT correspondence suggests a gauge-gravity duality in warped geometries [4]. Moreover, in string compactifications with fluxes, strongly warped metrics have proven very useful for moduli stabilization [5].

A strong space-time curvature is also beneficial when formulating lattice gravity at the level of an effective field theory (EFT) [6, 7, 8] (for related work see, *e.g.*, Ref. [9]). Although lattice gravity has, to lowest order in its interactions, a strong analogy to the gauge theory case [10, 11], it shows a radically different strong coupling behavior at the non-linear level. In 5D flat space, for instance, the ultraviolet (UV) strong coupling scale depends on the bulk volume, or infrared (IR) scale, via a so-called “UV/IR connection” that would forbid to take the large volume limit within a sensible EFT [7]. This UV/IR connection can, however, be avoided for discretized gravity in 5D warped space-time [12, 13] (for warped non-gravitational extra dimensions see, *e.g.*, Refs. [14, 15, 16])), which has been shown to work in the manifestly holographic regime and admits to take the large volume limit.

In this paper, we consider a six-dimensional (6D) lattice gravity setup, where the two extra dimensions are compactified on a discretized hyperbolic disk. We first analyze a coarse-grained latticization of the hyperbolic disk and show that the strong coupling scale in the UV is essentially set by the inverse disk radius and becomes independent of the total number of lattice sites on the boundary. We find that, even in the large volume limit, all bounds from laboratory experiments, astrophysics and cosmology on Kaluza-Klein (KK) gravitons are avoided and consider also collider implications of the model. In a second example, we study a fine-grained latticization of the hyperbolic disk with nonzero warping along the radial direction. We determine approximately the complete mass spectrum and the wave-function profiles of the gravitons. In the fine-grained model, we estimate a local strong coupling scale on the disk. We find that the presence of the 6th dimension can yield the theory on the discretized warped hyperbolic disk more weakly coupled than in the corresponding 5D warped case. In particular, the local strong coupling scale can become in the IR as large as the local Planck scale. We also analyze the action of a bulk right-handed neutrino in the coarse-grained model and find that a large curvature of the disk allows to generate small active Dirac neutrino masses via a volume suppression mechanism.

The paper is organized as follows. In Sec. 2, we introduce the extra-dimensional hyperbolic disk, that is then coarsely discretized in Sec. 3. Next, in Sec. 4, we calculate the strong coupling scale on the hyperbolic disk in the coarse-grained model. In Sec. 5, we analyze the EFT for the fine-grained latticization of the disk, which is warped along the radial direction, and show that the local strong coupling scale can be pushed to higher values by going from five to six dimensions on the hyperbolic disk. As an application, we present in Sec. 6 a mechanism for small Dirac neutrino masses in the coarse-grained model. Finally, in the Appendix, we derive the Fierz-Pauli Lagrangian on the hyperbolic disk.

¹For TeV-scale quantum gravity in flat extra dimension see Ref. [3].

2 6D warped hyperbolic space

Let us consider 6D general relativity compactified to four dimensions on an orbifold K_2/Z_2 , where K_2 is a two-dimensional hyperbolic disk of constant negative curvature. We use capital Roman indices $M = 0, 1, 2, 3, 5, 6$ to label the 6D coordinates x^M , while Greek indices $\mu = 0, 1, 2, 3$ denote the usual 4D coordinates x^μ . The 6D Minkowski metric is given by $\eta_{MN} = \text{diag}(1, -1, \dots, -1)$. A point on the hyperbolic disk K_2 is described by a pair of polar coordinates (r, φ) , where $r = x^5$ and $\varphi = x^6$ are the radial angular coordinates of the point, respectively; on K_2 , the coordinates r and φ can take the values $r \in [0, L]$, where $L \geq 0$ and $\varphi \in [0, 2\pi]$. We choose the coordinates such that r is the geodesic or proper distance of the point (r, φ) from the center, *i.e.*, L is the hyperbolic or proper radius of the disk. The orbifold K_2/Z_2 is obtained from K_2 by imposing on the angles φ the orbifold projection $\varphi \rightarrow -\varphi$, which restricts the physical space on the disk to $(r, \varphi) \in [0, L] \times [0, \pi]$.

We assume that the disk is warped along the radial direction like in the 5D RS scenario, where the radial coordinate r takes the role of the 5th dimension in the RS model. The 6D metric for the warped hyperbolic disk \tilde{g}_{MN} is given by the line element

$$ds^2 = e^{2\sigma(r)} g_{\mu\nu}(x, r, \varphi) dx^\mu dx^\nu - dr^2 - \frac{1}{v^2} \sinh^2(v \cdot r) d\varphi^2, \quad (1)$$

where $v > 0$ and $1/v$ is the curvature radius of the disk, $g_{\mu\nu}(x, r, \varphi)$ the 4D metric with $x \equiv (x^\mu)$, and

$$\sigma(r) = -w \cdot r, \quad (2)$$

where w is the curvature scale for the warping along the radial direction. We denote the components of the metric \tilde{g}_{MN} in Eq. (1) by $\tilde{g}_{\mu\nu} = e^{2\sigma(r)} g_{\mu\nu}(x, r, \varphi)$, $\tilde{g}_{55} = -1$ and $\tilde{g}_{66} = -v^{-2} \sinh^2(vr)$. This metric is defined for any values of $r \in [0, L]$, where the radius L of the disk is finite but can be taken arbitrarily large. Like in RS I, we have assumed in Eq. (1), orbifold boundary conditions with respect to r at the center $r = 0$ and the boundary $r = L$ of the disk. While we identify the UV brane with the center at $r = 0$, we have IR branes residing at the orbifold fixed points on the boundary at $r = L$. The orbifold K_2/Z_2 with the definition of the coordinates and the location of the UV and IR branes is shown in Fig. 3. In these coordinates, a concentric circle through a point (r, φ) has therefore a proper radius r and a proper circumference $2\pi v^{-1} \sinh(vr)$. The proper area of the corresponding disk is

$$A = \int dr d\varphi \sqrt{|\tilde{g}_{66}|} = 4\pi v^{-2} \sinh^2(vr/2). \quad (3)$$

For $vr \gg 1$, the circumference and the area of the circle thus grow exponentially with r .

It is interesting to compare our hyperbolic space with the Poincaré hyperbolic disk. Introducing a new radial coordinate \hat{r} that is defined by $dr = (1 - \frac{1}{4}v^2\hat{r}^2)^{-1}d\hat{r}$, leads from Eq. (1) to the Poincaré hyperbolic metric

$$ds^2 = e^{2\sigma(\hat{r})} g_{\mu\nu}(x, \hat{r}, \varphi) dx^\mu dx^\nu - \frac{1}{(1 - \frac{1}{4}v^2\hat{r}^2)^2} (d\hat{r}^2 + \hat{r}^2 d\varphi^2), \quad (4)$$

where $\sigma(\hat{r})$ is obtained by replacing in $\sigma(r) = -w \cdot r$ the coordinate r by $r(\hat{r})$. The metric in Eq. (4), has a coordinate singularity at $\hat{r} = 2/v$ corresponding to spatial infinity $r \rightarrow \infty$.

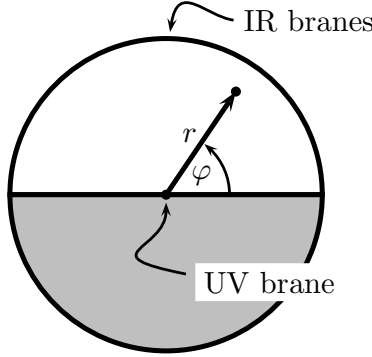


Figure 1: Physical space of the orbifold K_2/Z_2 . Shown are the coordinates (r, φ) of a point on the hyperbolic disk K_2 . The orbifold projection $\varphi \rightarrow -\varphi$, identifies the upper half of K_2 with the lower half (gray shaded region). The disk is warped along the radial direction, with the UV and IR branes located at the center and the boundary of the disk, respectively.

The coordinate \hat{r} is thus restricted to the interval $\hat{r} \in [0, 2/v]$, whereas $\varphi \in [0, 2\pi]$. The polar coordinates (\hat{r}, φ) define the Poincaré hyperbolic disk, which is shown in Fig. 2 for the example of a semi-regular $\{6, 6, 8\}$ tessellation. In Eq. (4), we have

$$\sigma(\hat{r}) = -\frac{w}{2v} \log \left(\frac{1 + v\hat{r}}{1 - v\hat{r}} \right). \quad (5)$$

In Fig. 2, the proper radius and proper circumference of a concentric circle through a point (\hat{r}, φ) are $-\sigma(\hat{r})/w$ and $2\pi\hat{r}/(1 - \frac{1}{4}v^2\hat{r}^2)$, which both diverge when approaching spatial infinity at $\hat{r} = 2/v$. In the rest of the paper, we will, however, always use the coordinates (r, φ) and take the metric as given in Eq. (1).

On the hyperbolic disk, we write the gravitational action as

$$\mathcal{S} = M_6^4 \int d^6x \sqrt{|\tilde{g}|} (\tilde{R} - 2\Lambda), \quad (6)$$

where $\tilde{g} \equiv \det \tilde{g}_{MN}$ and it is implied that the integration over r and φ is restricted to the hyperbolic disk. In Eq. (6), M_{6D} is the 6D Planck scale, Λ the bulk cosmological constant, and $\tilde{R} = \tilde{g}^{MN} \tilde{R}_{MN}$ is the 6D curvature scalar, where \tilde{R}_{MN} denotes the 6D Ricci tensor. The relevant parts of the action can be written in the form

$$\begin{aligned} \mathcal{S} = M_6^4 \int d^6x \sqrt{|g|} & \left[e^{2\sigma(r)} R_{4D} - \frac{1}{4} \tilde{g}^{55} \partial_r (e^{2\sigma(r)} g_{\mu\nu}) (g^{\mu\nu} g^{\alpha\beta} - g^{\mu\alpha} g^{\nu\beta}) \partial_r (e^{2\sigma(r)} g_{\alpha\beta}) \right. \\ & \left. - \frac{1}{4} \tilde{g}^{66} \partial_\varphi (e^{2\sigma(r)} g_{\mu\nu}) (g^{\mu\nu} g^{\alpha\beta} - g^{\mu\alpha} g^{\nu\beta}) \partial_\varphi (e^{2\sigma(r)} g_{\alpha\beta}) \right], \end{aligned} \quad (7)$$

where we have defined $|g| \equiv e^{-8\sigma(r)} |\tilde{g}|$ and R_{4D} is the 4D curvature scalar with respect to the 4D metric $g_{\mu\nu}$ (for a definition of R_{4D} and a complete derivation of Eq. (7) see Appendix A).

We expand $g_{\mu\nu}$ in terms of small fluctuations about 4D Minkowski space² by replacing $g_{\mu\nu} = \eta_{\mu\nu} + h_{\mu\nu}$. To quadratic order, the kinetic part of the graviton Lagrangian density is

²We also have $g^{\mu\nu} = \eta^{\mu\nu} - h^{\mu\nu} + h^{\mu\kappa} h_\kappa^\nu + \mathcal{O}(h_{\mu\nu}^3)$ and $h^{\mu\nu} \equiv \eta^{\mu\alpha} \eta^{\nu\beta} h_{\alpha\beta}$.

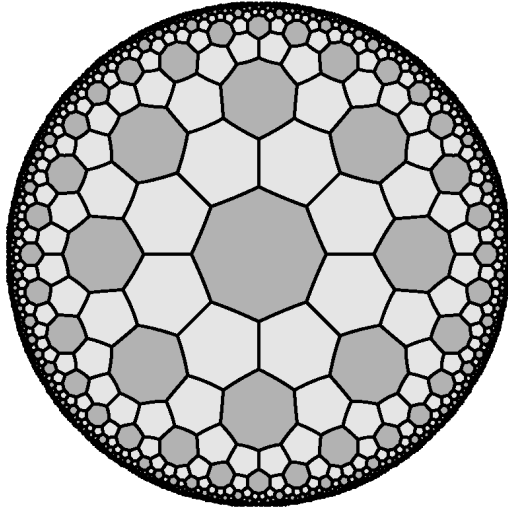


Figure 2: Poincaré hyperbolic disk with semi-regular $\{6,6,8\}$ tessellation [17].

then, after partial integration, explicitly found to be of the Fierz-Pauli form [18, 19]

$$\begin{aligned} \mathcal{S}_{\text{lin}} = & M_6^4 \int d^6x v^{-1} \sinh(vr) \left[\frac{1}{4} e^{2\sigma(r)} (\partial^\mu h^{\nu\kappa} \partial_\mu h_{\nu\kappa} - \partial^\mu h \partial_\mu h - 2h^\mu h_\mu + 2h^\mu \partial_\mu h) \right. \\ & + \frac{1}{4} e^{4\sigma(r)} (\partial_r h_{\mu\nu}) (\eta^{\mu\nu} \eta^{\alpha\beta} - \eta^{\mu\alpha} \eta^{\nu\beta}) (\partial_r h_{\alpha\beta}) \\ & \left. + \frac{1}{4} e^{4\sigma(r)} v^2 \sinh^{-2}(vr) (\partial_\varphi h_{\mu\nu}) (\eta^{\mu\nu} \eta^{\alpha\beta} - \eta^{\mu\alpha} \eta^{\nu\beta}) (\partial_\varphi h_{\alpha\beta}) \right], \end{aligned} \quad (8)$$

where $h = h^\mu_\mu$ and $h_\nu = \partial^\mu h_{\mu\nu}$. In the analysis of the 5D model in Ref. [7] it has proven useful to neglect the 4D vector, scalar and radion degrees of freedom. For simplicity, we have here also adopted a similar gauge, where we set $h_{5M} = h_{6M} = 0$ for $M = 0, 1, \dots, 6$.

Let us now consider the 6D Einstein tensor $\tilde{G}_{MN} = \tilde{R}_{MN} - \frac{1}{2}\tilde{g}_{MN}\tilde{R}$ for a flat 4D background $g_{\mu\nu} = \eta_{\mu\nu}$, in which case \tilde{G}_{MN} is on diagonal form $\tilde{G}_{MN} = \text{diag}(\tilde{G}_{11}, \tilde{G}_{22}, \dots, \tilde{G}_{66})$. Up to corrections of the order e^{-vr} , the components of \tilde{G}_{MN} asymptote in the IR very quickly to $\tilde{G}_{11} = \tilde{G}_{22} = \tilde{G}_{33} = -\tilde{G}_{00} = (3vw - 6w^2 - v^2)e^{-2wr}$, $\tilde{G}_{55} = 2vw - 6w^2$, and $\tilde{G}_{66} = -10w^2v^{-2}\sinh^2(vr)$. In this limit, the 6D Einstein equations can be formally satisfied (i) by adding to the gravitational action in Eq. (6) a “matter” action

$$\mathcal{S}_m = M_6^4 \int d^6x \sqrt{|\tilde{g}|} \tilde{g}^{AB} n_{AB}, \quad (9)$$

where n_{AB} denotes the tensor $n_{AB} \equiv -\tilde{G}_{AB}$ and (ii) by setting the bulk cosmological constant Λ in Eq. (6) equal to $\Lambda = -\frac{1}{2}\tilde{G}^A_A$. Note that for zero warping $w = 0$, we obtain the exact result that the tensor n_{AB} becomes constant throughout the bulk.

In what follows, we will view discrete gravitational extra dimensions as a tool to explore general relativity without the need to explicitly solve Einstein’s equations [12]. Here, the massive gravitons in the compactified theory can be understood in terms of a graph consisting of sites and links called “theory space”, and it is not necessary to find, *e.g.*, the gravitational source for an action of the type in Eq. (9).

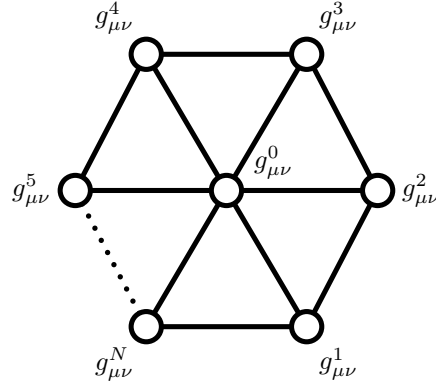


Figure 3: Coarse-grained discretization of the hyperbolic disk K_2 . The circles represent the sites and are labelled as $i = 0, 1, 2, \dots, N$. On each site i lives a graviton field $g_{\mu\nu}^i$ and two neighboring sites i and j are connected by a link $(i, j)_{\text{link}}$ (solid lines).

3 Coarse-grained discretization

In this section, we consider a discretization of the hyperbolic disk K_2 with metric as given in Eq. (1). In particular, we analyze here the case where the warping along the radial direction is set to zero $w = 0$, while having a non-vanishing curvature radius $v \neq 0$. The general case with both $w \neq 0$ and $v \neq 0$ will be studied later in Sec. 5.

3.1 Latticization

To discretize the hyperbolic disk K_2 , let us here choose the coarse-grained latticization as shown by the diagram in Fig. 3. The diagram is spanned by N sites located on the boundary of K_2 which are labelled as $i = 1, 2, \dots, N$, with the identification $i + N \equiv i$, while the center of the disk is represented by a single site $i = 0$. The sites on the boundary of K_2 are evenly spaced on a concentric circle with proper radius L around the central site $i = 0$ residing at the origin, *i.e.*, the i th site on the boundary has polar coordinates $(r, \varphi) = (L, i \cdot \Delta\varphi)$, where $\Delta\varphi = 2\pi/N$. In Fig. 3, two sites i and $i + 1$ on the boundary are connected by a link $(i, i + 1)_{\text{link}}$, while the site $i = 0$ in the center is connected to all N sites on the boundary by the links $(0, i)_{\text{link}}$. To implement a lattice gravity theory in terms of this triangulation, we will throughout interpret the sites and links following the theory for massive gravitons in Refs. [6, 7, 8]. Here, each site i is equipped with its own metric $g_{\mu\nu}^i$, which can be expanded about flat space as $g_{\mu\nu}^i = \eta_{\mu\nu} + h_{\mu\nu}^i$, where $\eta_{\mu\nu}$ is the usual 4D Minkowski metric. In a naive latticization of the linearized action \mathcal{S}_{lin} in Eq. (8) we then replace the derivatives on the sites as

$$\partial_\varphi h_{\mu\nu} \rightarrow \frac{1}{\Delta\varphi} (h_{\mu\nu}^{i+1} - h_{\mu\nu}^i), \quad \partial_r h_{\mu\nu} \rightarrow \frac{1}{L} (h_{\alpha\beta}^i - h_{\mu\nu}^0), \quad (10)$$

which gives the Fierz-Pauli graviton mass terms³

$$\begin{aligned} \mathcal{S}_{\text{FP}} = & M_4^2 \int d^4x \sum_{i=1}^N [m_*^2 (h_{\mu\nu}^i - h_{\mu\nu}^0) (\eta^{\mu\nu} \eta^{\alpha\beta} - \eta^{\mu\alpha} \eta^{\nu\beta}) (h_{\alpha\beta}^i - h_{\alpha\beta}^0) \\ & + m^2 (h_{\mu\nu}^{i+1} - h_{\mu\nu}^i) (\eta^{\mu\nu} \eta^{\alpha\beta} - \eta^{\mu\alpha} \eta^{\nu\beta}) (h_{\alpha\beta}^{i+1} - h_{\alpha\beta}^i)], \end{aligned} \quad (11)$$

where M_4 is the “local” universal 4D Planck scale on each of the sites, whereas m_* and respectively m denote the proper inverse lattice spacings in radial and angular direction. To relate M_4 to M_6 , we apply in Eq. (7) the discretization procedure given by

$$M_6^4 \int d^6x \sqrt{|\tilde{g}|} \rightarrow \frac{M_6^4 A}{N} \sum_{i=0,1}^N \int d^4x \sqrt{|g_4|}, \quad (12)$$

where A is the proper area of the disk from Eq. (3), with $r = L$, and $g_4 = \det g_{\mu\nu}$. In Eq. (12), it is understood that the sum starts from $i = 0$ for kinetic terms and from $i = 1$ for mass terms, respectively. The mass scales in Eq. (11) can then be matched as

$$m_* = \frac{1}{L}, \quad m = \frac{Nv}{2\pi \sinh(vL)}, \quad M_4^2 = \frac{M_6^4 A}{N}, \quad M_{\text{Pl}}^2 = M_6^4 A = M_4^2 N, \quad (13)$$

where $M_{\text{Pl}} \simeq 10^{18} \text{ GeV}$ is the usual 4D Planck scale of the low-energy theory. In the basis $(h_{\mu\nu}^0, h_{\mu\nu}^1, \dots, h_{\mu\nu}^N)$, the $(N+1) \times (N+1)$ graviton mass matrix reads

$$M_g^2 = m_*^2 \begin{pmatrix} N & -1 & -1 & \dots & -1 \\ -1 & 1 & & & \\ -1 & & 1 & & \\ \vdots & & & \ddots & \\ -1 & & & & 1 \end{pmatrix} + m^2 \begin{pmatrix} 0 & 0 & 0 & \dots & 0 \\ 0 & 2 & -1 & & -1 \\ 0 & -1 & 2 & \ddots & \\ \vdots & & \ddots & \ddots & -1 \\ 0 & -1 & & -1 & 2 \end{pmatrix}, \quad (14)$$

where the blank entries are zero. Diagonalization of M_g^2 leads to the graviton mass spectrum

$$M_0^2 = 0, \quad M_n^2 = m_*^2 + 4m^2 \sin^2 \frac{\pi n}{N}, \quad M_N^2 = (N+1)m_*^2, \quad (15)$$

where $n = 1, 2, \dots, N-1$. Note that the spectrum in Eq. (16) has been described previously for the gauge theory case [21, 22]. Denoting the n th mass eigenstate associated with a mass M_n as in Eq. (15) by $\hat{H}_{\mu\nu}^n$, the mass eigenstates can be written as

$$\hat{H}_{\mu\nu}^0 = \frac{1}{\sqrt{N+1}} (1, 1, 1, \dots, 1), \quad (16a)$$

$$\hat{H}_{\mu\nu}^n = \frac{1}{\sqrt{N}} (0, 1, e^{i\frac{2n\pi}{N}}, e^{i\frac{4n\pi}{N}}, \dots, e^{i\frac{2(N-1)n\pi}{N}}), \quad (16b)$$

$$\hat{H}_{\mu\nu}^N = \frac{1}{\sqrt{N(N+1)}} (N, -1, -1, \dots, -1), \quad (16c)$$

³For a recent discussion of Fierz-Pauli mass terms and ghosts in massive gravity see Ref. [20].

where in Eq. (16b) the index n runs over $n = 1, 2, \dots, N - 1$ and we have, for definiteness, taken N to be even. The mass eigenstates include a zero mode $\hat{H}_{\mu\nu}^0$ with flat profile. Note that the $N - 1$ massive eigenstates $\hat{H}_{\mu\nu}^n$ in Eq. (16b) are all exactly located on the boundary, while the N^{th} massive mode $\hat{H}_{\mu\nu}^N$ in Eq. (16c) is peaked in the center. The tower of masses M_n belonging to the states $\hat{H}_{\mu\nu}^n$ reproduces for $n \ll N$ a linear spectrum of KK modes of the order $m \cdot n/N$, that is sitting on top of m_*^2 . From Eq. (13) we finally observe that the limit $m \ll m_*$ can be realized even for $N \gg 1$ by a sufficiently large value of vL . In this case the $N - 1$ states in Eq. (16b) become practically degenerate with a mass m_* and the N^{th} mode $\hat{H}_{\mu\nu}^N$ becomes very heavy ($\gg m_*$).

3.2 Phenomenological implications

It has been recently demonstrated that large extra dimensions can be hidden in multi-throat configurations, where the occurrence of KK gravitons is delayed to energies that are much higher than the inverse radius of the extra dimension [23]. Such a multi-throat geometry is found in the coarse-grained model as a special case in the limit $m \rightarrow 0$. Thus, by the same arguments as in Ref. [23], the corrections to Newton's law in the coarse-grained model become only important, when the distance between two test masses is shorter than a critical radius $r_{\text{crit}} \simeq m_*^{-1} \log N$. For $N \simeq 10^{30}$, *e.g.*, we could thus have, like in large extra dimensions, the local Planck scale on the sites lowered down to $M_4 \simeq M_{\text{Pl}}/\sqrt{N} \simeq 1 \text{ TeV}$, while for $m_* \gtrsim 100 \text{ MeV}$ all current bounds on large extra dimensions from Cavendish-type experiments [24], astrophysics [25], and cosmology [26] are avoided.

The collider implications for the direct production of KK gravitons \hat{H}^n in $e^+ + e^- \rightarrow \gamma + \hat{H}^n$ and $p + p \rightarrow \text{jet} + \hat{H}^n$ reactions can be determined like in the large extra dimensional scenario: SM matter located on a site on the boundary has M_{Pl} suppressed couplings to the graviton zero mode and to the $N - 1$ quasi-degenerate modes, whereas the couplings to the heavy mode are even suppressed by a factor $\sqrt{N}M_{\text{Pl}}$. For example, assuming $N = 10^{30}$ sites and inverse lattice spacings $m_* = 14 \text{ TeV}$ and $m = 0.14 \text{ GeV}$, we find for a center-of-momentum energy $E_{\text{CoM}} = 14 \text{ TeV}$ and a quark energy $E_q \gtrsim 10^2 \text{ GeV}$, that the cross section for the production of an individual KK graviton via the process $q + g \rightarrow q + \hat{H}^n$ is $\sigma \sim 10^{-30} \text{ pb}$. This is, of course, not observable at a collider (as a detectability requirement of signal above background we take $\sigma \gtrsim 1 - 100 \text{ fb}$ [27]), but summing over the high multiplicity of $N = 10^{30}$ states, we actually have here a total cross section $\sigma_{\text{total}} \sim 1 \text{ pb}$, which could give a signal at the LHC. The signal would be a jet plus missing transverse energy. Of course, a proper treatment of this process should take into account the summation over the parton subprocesses, with the appropriate parton distribution functions, which is beyond the scope of this paper.

For a choice of parameters $N = 10^{30}$, $m_* = 1.0 \text{ TeV}$, $m = 1.0 \text{ GeV}$, $E_{\text{CoM}} = 1.0 \text{ TeV}$, and a lower cutoff for the photon energy of $E_\gamma \gtrsim 10 \text{ GeV}$, the cross section for the production of an individual KK mode via $e^+ + e^- \rightarrow \gamma + \hat{H}^n$ is $\sigma \sim 10^{-29} \text{ pb}$, resulting in a total cross section of the order $\sigma_{\text{total}} \sim 8 \text{ pb}$, which would, *e.g.*, be observable at the ILC. The signal would be a photon plus missing transverse energy. In Fig. 4, we give the cross sections for this reaction as a function of E_{CoM} . We give the results for $m_* = 1000 \text{ GeV}$, $m_* = 1250 \text{ GeV}$,

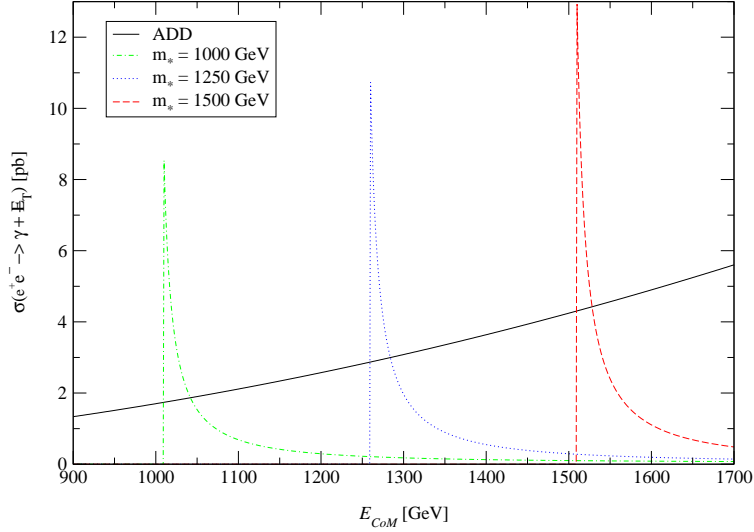


Figure 4: Cross section $\sigma(e^+ + e^- \rightarrow \gamma + \not{E}_T)$, in units of pb versus E_{CoM} in GeV. Given in the figure is the cross section for the disk model with $m_* = 1000$ GeV (dash-dotted), $m_* = 1250$ GeV (dotted), and $m_* = 1500$ GeV (dashed). In all cases, we have chosen $m = 1$ GeV and $N = 10^{30}$ sites. For comparison, we have also presented a typical ADD model with 2 extra dimensions and $M_f = 2.5$ TeV (solid line). We have also made a kinematic cut, by taking $E_\gamma \gtrsim 10$ GeV. The disk model gives a signal that is qualitatively different from usual large extra dimensions. The sharp peak close to $E_{\text{CoM}} \sim m_*$, is due to the nearly degenerate spectrum located around $E_{\text{CoM}} \sim m_*$. Below $E_{\text{CoM}} \sim m_*$, the cross section drops to zero, because of the mass-gap in the disk model.

and $m_* = 1500$ GeV. In all cases, we have chosen $N = 10^{30}$, $m = 1$ GeV and a lower cutoff for the photon energy of $E_\gamma \gtrsim 10$ GeV. We have also made a comparison with the ADD scenario [3] for 2 large extra dimensions and a fundamental scale $M_f = 2.5$ TeV. The coarse-grained model has a qualitatively different behavior compared to large extra dimensions. The sharp peak close to $E_{\text{CoM}} \sim m_*$, is due to the nearly degenerate spectrum, located around $E_{\text{CoM}} \sim m_*$. Below $E_{\text{CoM}} \sim m_*$, the cross section is zero, because of the large mass gap between the zero mode and the first excited mode.

In addition, the exchange of virtual KK modes could influence the cross sections for some SM processes, which we will, however, not discuss in further detail here.

4 Effective theory

In this section, we will study the strong coupling behavior of the coarse-grained model in Sec. 3.1, where we use throughout the EFT for massive gravitons introduced in Refs. [6, 7, 8]. Before turning to the complete latticized disk, it is instructive to consider the strong coupling scales in two of its sub-geometries. The first one is represented by the boundary of the disk, which we will call the “circle” geometry. The second one is obtained by removing the links on the boundary and we will henceforth call this theory space the “star” geometry.

4.1 Strong coupling in the circle geometry

To implement the EFT on the latticized hyperbolic disk K_2 , we replace in Eq. (10) the differences $h_{\mu\nu}^i - h_{\mu\nu}^j$ between the graviton fields on two sites i and j that are connected by a link $(i, j)_{\text{link}}$ by

$$h_{\mu\nu}^i - h_{\mu\nu}^j \rightarrow g_{\mu\nu}^i - \partial_\mu Y_{ij}^\alpha \partial_\nu Y_{ij}^\beta g_{\alpha\beta}^j, \quad (17a)$$

with the link fields

$$Y_{ij}^\mu(x_\mu) = x^\mu + A_{ij}^\mu(x_\mu) + \partial^\mu \phi_{ij}(x_\mu), \quad (17b)$$

where the fields A_{ij}^μ and ϕ_{ij} represent the vector and scalar components of the Goldstone bosons that restore general coordinate invariances in the EFT. For a detailed description of the technique for restoring general coordinate invariances, see Refs. [6, 7, 8].

The circle geometry is obtained from the coarse-grained latticized disk in Sec. 3.1 by assuming $m_* = 0$ and m nonzero. Since this reduces the model to the 5D lattice gravity theory discussed in Ref. [7], we will only give a short review of this case here.

The kinetic Lagrangian of the gravitons is found by specializing in Eq. (17) the links $(i, j)_{\text{link}}$ to the case $(i, j)_{\text{link}} = (i, i-1)_{\text{link}}$, where $i = 2, \dots, N, N+1$. As a consequence, we obtain for the discrete circle geometry from the Fierz-Pauli mass term in Eq. (11) the action

$$\mathcal{S}_{\text{circle}} = \mathcal{S}_{\text{FP}} + \int d^4x M_4^2 \sum_{i=1}^N (h_{\mu\nu}^i \square h_{\mu\nu}^i + m^2 [(h_{\mu\nu}^i - h_{\mu\nu}^{i-1}) \square \phi_{i,i-1} + (\square \phi_{i,i-1})^3]). \quad (18)$$

The kinetic mixing between the gravitons and scalar Goldstones can be eliminated by partial integration and a subsequent Weyl rescaling, which produces proper kinetic terms for the Goldstones [6]. As shown in Ref. [7], this EFT for massive gravitons has a cutoff

$$\Lambda_{\text{circle}} = (M_4 m^4 / N^{5/2})^{1/5} = (M_{\text{Pl}} m^4 / N^3)^{1/5}, \quad (19)$$

where we have used that the usual 4D Planck scale $M_{\text{Pl}} \simeq 10^{18}$ GeV is related to the local 4D Planck scale on the sites M_4 by $M_{\text{Pl}} = \sqrt{N} M_4$ (see Eq. (13)). The strong coupling scale Λ_{circle} depends on the number of lattice sites N , *i.e.*, the circumference $R = N m^{-1}$ of the circle. The fact that the UV scale Λ_{circle} depends on the IR scale R has been called UV/IR connection and restricts in a sensible EFT the possible number of sites to a maximal value $N_{\text{max}} = (M_4^2 m R^3)^{1/8}$ [7].

4.2 Strong coupling in the star geometry

The star geometry arises from the disk model by setting the parameters $m = 0$ and $m_* \neq 0$. Note that this geometry is similar to the multi-throat configuration, which has been analyzed for the gauge theory case in Ref. [23]. In contrast to Sec. 4.1, we specialize here to the case in which the links $(i, j)_{\text{link}}$ in Eq. (17) are $(i, j)_{\text{link}} = (i, 0)_{\text{link}}$, where $i = 1, 2, \dots, N$. We then obtain from the Fierz-Pauli mass term in Eq. (11) the action

$$\mathcal{S}_{\text{star}} = \mathcal{S}_{\text{FP}} + \int d^4x M_4^2 (h_{\mu\nu}^0 \square h_{\mu\nu}^0 + \sum_{i=1}^N (h_{\mu\nu}^i \square h_{\mu\nu}^i + m_*^2 [(h_{\mu\nu}^0 - h_{\mu\nu}^i) \square \phi_{0,i} + (\square \phi_{0,i})^3])), \quad (20)$$

where we have also included the kinetic terms of the gravitons. In Eq. (20), the terms $m_*^2(h_{\mu\nu}^0 - h_{\mu\nu}^i)\square\phi_{0,i}$ can be written as a $(N+1) \times N$ kinetic matrix, which is proportional to

$$\begin{pmatrix} 1 & 1 & 1 & \dots & 1 \\ -1 & 0 & 0 & \dots & 0 \\ 0 & -1 & 0 & \dots & 0 \\ 0 & 0 & -1 & \dots & 0 \\ \vdots & \vdots & \vdots & \ddots & \vdots \\ 0 & 0 & 0 & \dots & -1 \end{pmatrix}, \quad (21)$$

where the rows and columns are spanned by $(h_{\mu\nu}^0, h_{\mu\nu}^1, \dots, h_{\mu\nu}^N)$ and $(\phi_{0,1}, \phi_{0,2}, \dots, \phi_{0,N})$, respectively. To determine here the strong coupling scale, we express the gravitons on the boundary as the linear combinations $h_{\mu\nu}^i = \frac{1}{\sqrt{N}} \sum_{n=1}^N e^{i2\pi i \cdot n/N} H_{\mu\nu}^n$, where we have introduced the fields $H_{\mu\nu}^n = H_{\mu\nu}^n$ for $n = 2, 3, \dots, N-1$ with $H_{\mu\nu}^n$ from Eq. (16b) and $H_{\mu\nu}^N$ is in the basis of Eqs. (16) given by the $(N+1)$ -component vector $H_{\mu\nu}^N = \frac{1}{\sqrt{N}}(0, 1, 1, \dots, 1)$. Similarly, we expand the scalar components of the Goldstone fields belonging to the links $(i, 0)$ as $\phi_{i,0} = \frac{1}{\sqrt{N}} \sum_{n=1}^N e^{i2\pi i \cdot n/N} \Phi_n$. The matrix in Eq. (21) gets then transformed to

$$\begin{pmatrix} 0 & 0 & 0 & \dots & \sqrt{N} \\ -1 & 0 & 0 & \dots & 0 \\ 0 & -1 & 0 & \dots & 0 \\ 0 & 0 & -1 & \dots & 0 \\ \vdots & \vdots & \vdots & \ddots & \vdots \\ 0 & 0 & 0 & \dots & -1 \end{pmatrix}, \quad (22)$$

where the rows and columns have been written in the bases $(h_{\mu\nu}^0, H_{\mu\nu}^1, H_{\mu\nu}^2, \dots, H_{\mu\nu}^N)$ and $(\Phi_1, \Phi_2, \dots, \Phi_N)$, respectively. Let us next perform a rotation by the angle $\arctan(\sqrt{N})$ acting in the 2-dimensional subspace $(h_{\mu\nu}^0, H_{\mu\nu}^N)$ from the left on the first and last rows of the matrix in Eq. (22). This rotates away the entry \sqrt{N} in the top-right corner and introduces new basis vectors via $(h_{\mu\nu}^0, H_{\mu\nu}^N) \rightarrow (H_{\mu\nu}^0, H_{\mu\nu}^N)$, with $H_{\mu\nu}^0$ and $H_{\mu\nu}^N$ as defined in Eqs. (16a) and (16b), respectively. We can then approximate the action in Eq. (20) by

$$\begin{aligned} \mathcal{S}_{\text{star}} &= \mathcal{S}_{\text{FP}} + \int d^4x M_4^2 \left[h_{\mu\nu}^0 \square h_{\mu\nu}^0 + \sum_{n=1}^N \left(H_{\mu\nu}^n \square H_{\mu\nu}^{-n} \right. \right. \\ &\quad \left. \left. - m_*^2 H_{\mu\nu}^n \square \Phi_{-n} \right) + \sum_{n,m=1}^N \left(\frac{m_*^2}{\sqrt{N}} (\square \Phi_n)(\square \Phi_m)(\square \Phi_{-n-m}) \right) \right], \end{aligned} \quad (23)$$

where we have defined $H_{\mu\nu}^{-n} = H_{\mu\nu}^{N-n}$ and $\Phi_{-n} = \Phi_{N-n}$. From this equation, we read off the graviton fields in canonical normalization $\hat{H}_{\mu\nu}^n = M_4 H_{\mu\nu}^n$ and, consequently, the canonically normalized scalar Goldstone modes are $\hat{\Phi}_n = M_4 m_*^2 \Phi_n$. In Eq. (23), we thus have

$$M_4^2 m_*^2 (\square \Phi_n)(\square \Phi_m)(\square \Phi_{-n-m}) = \frac{1}{\sqrt{N} M_4 m_*^4} (\square \hat{\Phi}_n)(\square \hat{\Phi}_m)(\square \hat{\Phi}_{-n-m}). \quad (24)$$

From the amplitude for $\hat{\Phi}_n - \hat{\Phi}_m$ scattering, we hence find for the star geometry the strong coupling scale

$$\Lambda_{\text{star}} = (\sqrt{N} M_4 m_*^4)^{1/5} = (M_{\text{Pl}} m_*^4)^{1/5}, \quad (25)$$

which is independent from the number of sites N on the boundary. Therefore, the UV/IR connection problem from the circle geometry is absent in the star geometry. Note that the strong coupling scale in Eq. (25) is what we would expect in the theory of a single graviton with mass m_* [6].

4.3 Strong coupling on the disk

In the disk model of Sec. 3.1, the links form a mesh which would generally imply the presence of additional uneaten pseudo-Nambu-Goldstone bosons. These bosons, however, can acquire large masses from invariant plaquette terms that are added to the action [6]. In our model, we will therefore assume that these scalars decouple and estimate the strong coupling scale on the disk Λ_{disk} only from the scattering of the modes that are eaten by the gravitons.

The combination of $\mathcal{S}_{\text{circle}}$ and $\mathcal{S}_{\text{star}}$ gives, using the notation of Sec. 4.2, in momentum basis the total action of the disk

$$\begin{aligned} \mathcal{S}_{\text{disk}} = & \mathcal{S}_{\text{FP}} + \int d^4x M_4^2 \left[h_{\mu\nu}^0 \square h_{\mu\nu}^0 + \sum_{n=1}^N \left(H_{\mu\nu}^n \square H_{\mu\nu}^{-n} \right. \right. \\ & - H_{\mu\nu}^n \square (m_*^2 \Phi_{-n} + m^2 (1 - e^{-i2\pi\cdot n/N}) \Phi'_{-n}) \Big) \\ & + \left. \sum_{n,k=1}^N \left(\frac{m_*^2}{\sqrt{N}} (\square \Phi_n) (\square \Phi_k) (\square \Phi_{-n-k}) + \frac{m^2}{\sqrt{N}} (\square \Phi'_n) (\square \Phi'_k) (\square \Phi'_{-n-k}) \right) \right], \end{aligned} \quad (26)$$

where Φ_n and $H_{\mu\nu}^n$ are defined as in Eq. (23), while Φ'_n is related to the scalar Goldstone $\phi_{i,i-1}$ of the circle geometry by $\phi_{i,i-1} = \frac{1}{\sqrt{N}} \sum_{n=1}^N e^{i2\pi i \cdot n/N} \Phi'_n$. From Eq. (26) we thus find that for $n \ll N$ the Goldstones Φ_n^0 which become the scalar longitudinal components of the the $H_{\mu\nu}^n$ are approximately given by

$$\Phi_n^0 \approx m_*^2 \Phi_n + 2\pi \frac{n}{N} m^2 \Phi'_n. \quad (27)$$

For large N , the field Φ_n^0 becomes dominantly composed of Φ_n , whereas Φ'_n makes up almost entirely the uneaten linear combination orthogonal to Φ_n^0 . Consider now in Eq. (26) the tri-linear derivative coupling term involving the field Φ'_n . In the pure circle geometry discussed in Sec. 4.1, the coupling of this term becomes strong for large N and is responsible for the UV/IR connection. In our disk model, however, the linear combination orthogonal to Φ_n^0 decouples. In this limit, since the admixture of Φ'_n to Φ_n^0 is only of the order $\sim 1/N$, the tri-linear coupling of Φ'_n in Eq. (26) picks up a suppression factor $\sim 1/N^3$, when expressed in terms of the canonically normalized fields $\hat{\Phi}_n^0 = M_4 \Phi_n^0$, and takes approximately the form

$$\frac{m^2}{\sqrt{N}} (\square \Phi'_n) (\square \Phi'_k) (\square \Phi'_{-n-k}) \rightarrow \frac{m^8}{N^{7/2} M_4 m_*^{12}} (\square \hat{\Phi}_n^0) (\square \hat{\Phi}_k^0) (\square \hat{\Phi}_{-n-k}^0), \quad (28)$$

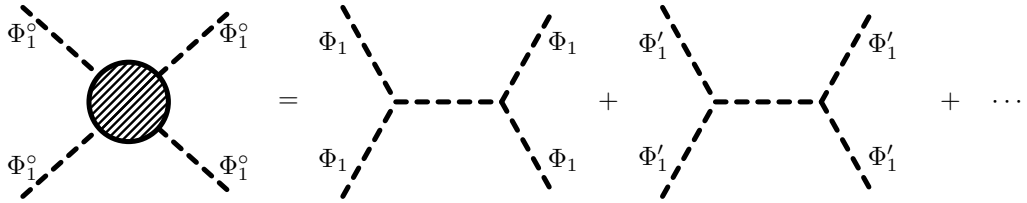


Figure 5: Contributions to the scattering amplitude of the lightest massive graviton in the disk model. For large N , the scalar Φ_1^o is dominantly composed of Φ_1 and the relative contribution from $\Phi'_1 - \Phi_1'$ scattering becomes suppressed by a factor $\sim 1/N^6$.

where we have assumed that $n, k \sim 1 \ll N$. Unless m is not too large compared to m_* , the dominant contribution to the massive graviton scattering is therefore given by the first tri-linear derivative coupling in the third line in Eq. (26) (see Fig. 5). This coupling is similar to the term in Eq. (23) that sets the strong coupling scale in the star geometry. For $N \rightarrow \infty$, the strong coupling scale of the disk model Λ_{disk} thus converges to

$$\Lambda_{\text{disk}} \rightarrow \Lambda_{\text{star}} = (M_{\text{Pl}} m_*^4)^{1/5}. \quad (29)$$

The EFT for massive gravitons in our disk model does therefore not suffer from the UV/IR connection of the circle sub-geometry and thus allows to take the large N limit. Instead, the strong coupling scale on the disk is similar to that of the theory of a single massive graviton.

5 Fine-grained discretization

In this section, we will consider a refinement of the discretization of the hyperbolic disk discussed in Sec. 3. Different from our earlier discussion, we now assume that the disk is strongly warped along the radial direction.

5.1 Structure of the graph

In choosing a refined discretization of the hyperbolic disk, we will, in what follows, confine ourselves to the class of graphs that are collectively represented by Fig. 6, where the sites and links are interpreted as in Sec. 3.1. The sites are placed on concentric circles (dashed lines) around a site in the center of the disk. Starting from the innermost circle and going outward, the circles are labelled as $k = 1, 2, \dots, k_{\text{max}}$, where we identify the outermost circle labelled as k_{max} with the boundary of the disk. Fig. 6 depicts the special case $k_{\text{max}} = 4$.

Let us now specify the structure of the graph in more detail. We distinguish between two types of links: ‘‘angular’’ and ‘‘radial’’ links. In Fig. 6, the angular links connect neighboring sites on the same circle and are shown as dashed curved lines; the radial links connect neighboring sites that are not on the same circle and are drawn as solid straight lines.

The site in the center is connected with ℓ radial links to the sites on the first circle. Every site on the k th circle, where $1 \leq k < k_{\text{max}}$, is connected by ℓ radial links to the nearest ℓ sites on the next outer circle with label $k + 1$. In Fig. 6, we have $\ell = 2$. To maximize the symmetry of the graph, we assume that all sites on a circle are evenly spaced and that the

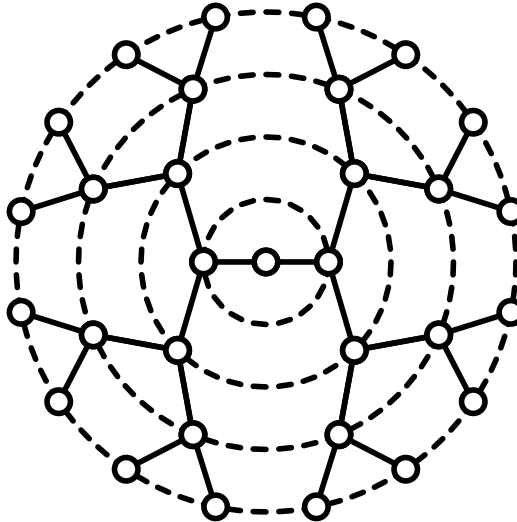


Figure 6: Fine-grained discretization of the hyperbolic disk. The graph shows the special case $\ell = 2$ and $k_{\max} = 4$. Angular links are shown as dashed lines and radial links as solid lines.

links emanating outward from any given site on some inner circle with label $k < k_{\max}$, are always symmetrically arranged with respect to a 2-fold mirror symmetry axis through this site and the center of the disk. In what follows, we will, for simplicity, and unless otherwise mentioned, specialize to the case $\ell = 2$ as in Fig. 6 but leave k_{\max} a free positive integer parameter. The generalization to $\ell > 2$ is then straightforward. On the k th circle, we hence have $N_k \equiv 2^k$ sites and the total number of sites on the first k circles is $N_k^{\text{total}} \equiv 2^{k+1} - 1$. For later notational convenience, we denote by $N_0^{\text{total}} = N_0 = 1$ the number of sites in the center. The exponential growth of lattice sites when moving from the center outward on the disk is a salient feature of our graph, that will play an important role in the EFT.

Similar to the 5D case in Ref. [12], we assume that the radial geodesic coordinates of the sites are integer multiples of a common proper radial lattice spacing a_r , and take the values

$$r_k = k \cdot a_r, \quad (30)$$

where $k = 0, 1, 2, \dots, k_{\max}$, *i.e.*, the k th circle has a proper radius r_k . We define m_* as the inverse radial lattice spacing $m_* \equiv 1/a_r$. Since the sites on each circle are evenly spaced, we define the lattice spacing in φ direction between two neighboring sites on the k th circle by $a_{\varphi,k} = 2\pi \sinh(vr_k)/(vN_k)$, where $2\pi \sinh(vr_k)/v$ is the proper circumference of the k th circle and $m_k = 1/a_{\varphi,k}$ is the inverse lattice spacing on this circle. The inverse lattice spacing will be written as $m_k \equiv 1/a_{\varphi,k}$, which is in general k -dependent.

To simplify further the discussion as much as possible, we will, in what follows, go to an approximation in which all radial links have the same universal proper length a_r . This is, of course, an arbitrarily good approximation for the set of radial links that radiate outward from the k th circle for large $k \gg 1$ and small curvature radius $vL \ll 1$. However, in our approximation, we even assume that all the $N_k^{\text{total}} - 1$ radial links on the disk have a common proper length a_r , irrespective of their position on the disk or the size of the curvature radius.

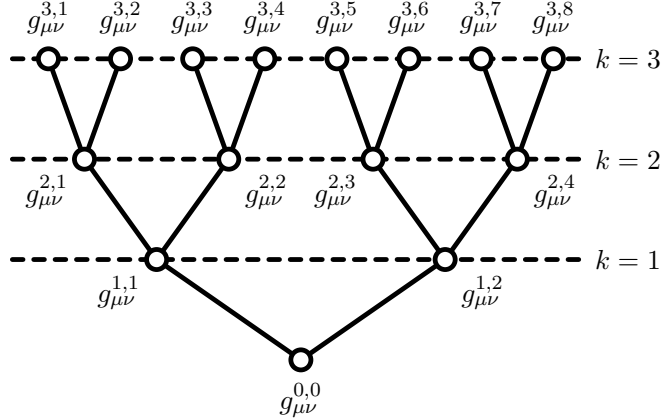


Figure 7: Sub-graph of the discretized hyperbolic disk obtained by truncating the disk at $k_{\max} = 3$. The horizontal dashed lines represent segments from the concentric circles with labels $k = 1, 2, 3$. The labeling of the sites by (k, i) is made explicit for the associated metrics $g_{\mu\nu}^{k,i}$ (see text).

5.2 Radial warping

Let us now consider the implementation of a nonzero warping along the radial direction of the refined discretized hyperbolic disk introduced in Sec. 5.1. The graph we are concerned with, is of the type given in Fig. 6, where the number of circles k_{\max} can be arbitrary. In this section, we will, for simplicity, neglect the effect of the angular links (dashed lines) and assume that the graviton masses are generated only by the radial links (solid lines). As we will show in Sec. 5.5, the angular links can be easily taken into account in full generality for the complete disk model and do not have significant impact on the relevant properties of the model with radial links only.

Each site on the disk can be specified by an index pair (k, j) , where k is the label of the circle where the site is located and $j = 1, 2, \dots, N_k$ labels (e.g., in clockwise direction) all the sites on this circle. The site in the center carries the index pair $(0, 0)$. The metric living on the site (k, j) is written as $g_{\mu\nu}^{k,j} = \eta_{\mu\nu} + h_{\mu\nu}^{k,j}$, where $h_{\mu\nu}^{k,j}$ is the graviton field on this site. We adopt a similar notation in momentum space and denote the canonically normalized graviton mass eigenstates by $\hat{H}_{\mu\nu}^{k,j}$, where $k = 1, 2, \dots, k_{\max}$ and $j = 1, 2, \dots, N_k$, while $H_{\mu\nu}^{0,0}$ is the zero mode. The mass eigenvalue belonging to $\hat{H}_{\mu\nu}^{k,i}$ will be denoted by $\lambda_{k,i}$.

To specify the labelling of the sites more exactly, consider Fig. 7, which is another way of representing the inner part of the disk in Fig. 6, where the center appears now at the bottom of the graph and the concentric circles are shown as dashed horizontal lines. The radial links are again drawn as straight solid lines. In the above notation, any given site (k, i) on the k th circle, where $k = 0, 1, 2, \dots, k_{\max} - 1$, is connected via two radial links with two nearest neighboring sites $(k+1, j_1)$ and $(k+1, j_2)$ on the next outer circle. The indices j_1 and j_2 are recursively defined as functions of the index i by setting $j_1 = 2(i-1) + 1$ and $j_2 = 2(i-1) + 2$. Starting with the label $(0, 0)$ for the center, this prescription fixes completely the assignment of labels for all sites on the circle by requiring the indices i in (k, i) to be ordered, e.g., in clockwise direction on the disk. This labelling is shown explicitly

in Fig. 7 for the fields $g_{\mu\nu}^{k,i}$ living on the sites (k, i) .

To introduce the warping along the radial direction of the fine-grained latticized disk, we proceed exactly like in the discretized 5D RS model in Ref. [12] and replace in the linearized gravitational action in Eq. (8), *e.g.*, the derivatives in the r direction by

$$e^{-4wr} \partial_r h_{\mu\nu} \rightarrow \frac{1}{a_r^2} e^{-4wkar} (h_{\mu\nu}^{k,j} - h_{\mu\nu}^{k-1,i}), \quad (31)$$

where it is understood that the sites $(k-1, i)$ and (k, j) , with $k = 1, 2, \dots, k_{\max}$, are nearest neighbors on adjacent circles connected by a radial link. It is convenient to introduce a dimensionless number $\epsilon < 1$, which is related to the warp factor by $\epsilon \equiv e^{-war}$. Since from each site in the interior of the disk exactly two radial links are pointing outward, the index j in Eq. (31) can be either $j = 2(i-1) + 1$ or $j = 2(i-1) + 2$. We thus obtain for the discretized action on the warped hyperbolic disk

$$\mathcal{S}_{\text{lin}} = \int d^4x M_4^2 \sum_{k=0}^{k_{\max}} \sum_{i=1}^{N_k} \epsilon^{2k} h_{\mu\nu}^{k,i} \square h_{\mu\nu}^{k,i} + \mathcal{S}_{\text{FP}}, \quad (32)$$

where \mathcal{S}_{FP} are the Fierz-Pauli mass terms

$$\begin{aligned} \mathcal{S}_{\text{FP}} = & M_4^2 \int d^4x \sum_{k=1}^{k_{\max}} \sum_{i=1}^{N_{k-1}} m_*^2 \epsilon^{4k} \left[(h_{\mu\nu}^{k-1,i} - h_{\mu\nu}^{k,n_i}) (\eta^{\mu\nu} \eta^{\alpha\beta} - \eta^{\mu\alpha} \eta^{\nu\beta}) (h_{\alpha\beta}^{k-1,i} - h_{\alpha\beta}^{k,n_i}) \right. \\ & \left. + (h_{\mu\nu}^{k-1,i} - h_{\mu\nu}^{k,n_i+1}) (\eta^{\mu\nu} \eta^{\alpha\beta} - \eta^{\mu\alpha} \eta^{\nu\beta}) (h_{\alpha\beta}^{k-1,i} - h_{\alpha\beta}^{k,n_i+1}) \right], \end{aligned} \quad (33)$$

in which the index n_i on the k th circle is a function of the index i on the next inner circle and reads $n_i = 2(i-1) + 1$, where $i = 1, 2, \dots, N_{k-1}$. From the kinetic terms in Eq. (32), we find that $M_k \equiv M_4 \epsilon^k$ is the local Planck scale on each site on the k th circle. In the basis of canonically normalized fields $\hat{h}_{\mu\nu}^{k,i} = M_4 \epsilon^k h_{\mu\nu}^{k,i}$, the Fierz-Pauli mass terms then lead to the graviton mass matrix

$$M_{(k,i)(l,j)} = \frac{1}{a_r^2} \epsilon^{2(l-1)} [(\epsilon^2 + \epsilon^{-2}) \delta_{kl} \delta_{ij} - \epsilon^{-1} \delta_{k+1,l} (\delta_{n_i j} + \delta_{n_{i+1} j}) - \epsilon \delta_{k-1,l} \delta_{n_i i}], \quad (34)$$

where $M_{(k,i)(l,j)}$ is the mass matrix element between $\hat{h}_{\mu\nu}^{k,i}$ and $\hat{h}_{\mu\nu}^{l,j}$, while n_i is defined as in Eq. (33). In what follows, we will work in the “rough, local flat space approximation” of Ref. [12], where the product $w \cdot a_r$, entering the warp factor, is moderately small, *i.e.*, $war < 1$. In this approximation, the mass matrix in Eq. (34) reduces to

$$M_{(k,i)(l,j)} \approx \frac{1}{a_r^2} \epsilon^{2l} [2 \delta_{kl} \delta_{ij} - \delta_{k+1,l} (\delta_{n_i j} + \delta_{n_{i+1} j}) - \delta_{k-1,l} \delta_{n_i i}]. \quad (35)$$

To arrive at Eq. (35), we have set in Eq. (34) $\epsilon, \epsilon^2 = 1$, but kept the higher powers ϵ^{2l} , which can be small for $l \gg 1$. Note, that this mass matrix is what one would expect in the corresponding gauge theory case [14, 15, 16].

Let us now comment on the range of parameters we are interested in. Like in the RS scenario, we will assume that the usual 4D low energy Planck scale $M_{\text{Pl}} \simeq 10^{18} \text{ GeV}$ is

given by the local Planck scale M_4 on the UV brane, *i.e.*, we set $M_4 = M_{\text{Pl}}$, which holds approximately as long as $\epsilon \cdot \ell \ll 1$, say, if $\epsilon \cdot \ell \lesssim 0.5$. For definiteness, we take also the inverse radial lattice spacing $m_* = 1/a_r$ to be of the order $m_* = M_4$, and assume that the small expansion parameter is $\epsilon \simeq 0.1$. Furthermore, we suppose that the curvature scale for the warping is somewhat smaller than the fundamental scale $w \simeq (0.1) \times M_{\text{Pl}}$. To realize, *e.g.*, the RS I model [1] with the SM on one of the sites on the boundary of the disk, we need on the boundary a local Planck scale $M_{k_{\text{max}}} = \epsilon^{k_{\text{max}}} M_{\text{Pl}} \simeq 1 \text{ TeV}$, which implies that the disk has a proper radius, which is roughly $k_{\text{max}} \simeq 15$ Planck units M_{Pl}^{-1} wide. For our special case with $\ell = 2$, we would then have $N_{k_{\text{max}}} = 3 \times 10^4$ sites on the boundary.

5.3 Spectrum for a subgraph

Before analyzing the masses and eigenstates of the gravitons in the model for an arbitrary number of circles k_{max} , let us first study the spectrum for the subgraph in Fig. 7. From Eq. (35), we find in the basis $(\hat{h}_{\mu\nu}^{0,0}, \hat{h}_{\mu\nu}^{1,1}, \hat{h}_{\mu\nu}^{1,2}, \hat{h}_{\mu\nu}^{2,1}, \hat{h}_{\mu\nu}^{2,2}, \hat{h}_{\mu\nu}^{2,3}, \hat{h}_{\mu\nu}^{2,4})$ for the graviton mass matrix

$$M_g^2 = m_*^2 \epsilon^{2k} \begin{pmatrix} 2 & -1 & -1 & 0 & 0 & 0 & 0 \\ -1 & 1 + 2\epsilon^2 & 0 & -\epsilon^2 & -\epsilon^2 & 0 & 0 \\ -1 & 0 & 1 + 2\epsilon^2 & 0 & 0 & -\epsilon^2 & -\epsilon^2 \\ 0 & -\epsilon^2 & 0 & \epsilon^2 & 0 & 0 & 0 \\ 0 & -\epsilon^2 & 0 & 0 & \epsilon^2 & 0 & 0 \\ 0 & 0 & -\epsilon^2 & 0 & 0 & \epsilon^2 & 0 \\ 0 & 0 & -\epsilon^2 & 0 & 0 & 0 & \epsilon^2 \end{pmatrix}, \quad (36)$$

where we have truncated the graph in Fig. 7 at the dashed line labelled by $k = 2$. In what follows, we will determine the masses and mass eigenstates of the gravitons to leading order in perturbation theory following the example of the warped gauge theory case in Refs. [14, 23].

In the following, we choose a convention where the mass eigenvalue $\lambda_{k,i}$ belonging to $\hat{H}_{\mu\nu}^{k,i}$ measures the actual mass in multiples of $m_*^2 \epsilon^{2(k-1)}$. The mass eigenstates of the matrix in Eq. (36) contain a flat zero mode

$$\hat{H}_{\mu\nu}^{0,0} = \frac{1}{\sqrt{7}}(1, 1, 1, 1, 1, 1, 1) \quad : \quad \lambda_{0,0} = 0, \quad (37a)$$

and two heavy modes

$$\hat{H}_{\mu\nu}^{1,1} = \frac{1}{\sqrt{2}}(0, -1, 1, 0, 0, 0, 0) \quad : \quad \lambda_{1,1} = \epsilon^2, \quad (37b)$$

$$\hat{H}_{\mu\nu}^{1,2} = \frac{1}{\sqrt{6}}(-2, 1, 1, 0, 0, 0, 0) \quad : \quad \lambda_{1,2} = 3\epsilon^2, \quad (37c)$$

where we have listed in each line also the eigenvalue corresponding to each eigenstate. Observe that the zero mode has an exactly flat wave-function profile, whereas the two heavy modes are more localized toward the center of the disk. Furthermore, the spectrum contains the following three degenerate states

$$\hat{H}_{\mu\nu}^{2,j} = \frac{1}{2}(0, 0, 0, 1, e^{i2\pi j/4}, e^{i4\pi j/4}, e^{i6\pi j/4}) \quad : \quad \lambda_{2,j} = \epsilon^4, \quad (37d)$$

where $j = 1, 2, 3$, as well as the slightly heavier mode

$$\hat{H}_{\mu\nu}^{2,4} = \frac{1}{\sqrt{84}}(-4, -4, -4, 3, 3, 3, 3) \quad : \quad \lambda_{2,4} = \frac{7}{3}\epsilon^4. \quad (37e)$$

It is important to note that this mode profile and the flat profile of the zero mode $\hat{H}_{\mu\nu}^{0,0}$ in Eq. (37a) are only a result of going to the rough, local flat space approximation in Eq. (35). We will discuss the differences to the exact profiles in the following section.

5.4 Spectrum for the general case

Let us now consider the graviton spectrum for an arbitrary number of concentric circles k_{\max} in the rough, local flat space approximation of Sec. 5.2. We determine the eigenvalues and eigenstates of the graviton mass matrix to leading order in perturbation like in Sec. 5.2. With the definition of the proper radial lattice spacing in Eq. (30), we thus find that the graviton mass matrix has a flat zero mode

$$\hat{H}_{\mu\nu}^{0,0} = \frac{1}{\sqrt{N_{k_{\max}}^{\text{total}}}}(1, 1, \dots, 1) \quad : \quad \lambda_{0,0} = 0, \quad (38)$$

and one degenerate mode

$$\hat{H}_{\mu\nu}^{1,1} = \frac{1}{\sqrt{2}}(0, 1, e^{i\pi}, 0, \dots, 0) \quad : \quad \lambda_{1,1} = \epsilon^2. \quad (39)$$

In addition, we have a slightly heavier mode with eigenvalue $\lambda_{1,2} = 3\epsilon^2$ that reads

$$\hat{H}_{\mu\nu}^{1,2} = \frac{1}{\sqrt{6}}(-2, 1, 1, 0, \dots, 0) \quad : \quad \lambda_{1,2} = 3\epsilon^2. \quad (40)$$

Generally, for each $k = 2, 3, \dots, k_{\max}$, there are in total $N_k - 1$ degenerate modes that are given by

$$\hat{H}_{\mu\nu}^{k,j} = \frac{1}{\sqrt{N_k}} \underbrace{(0, \dots, 0, 1, e^{i2\pi j/N_k}, e^{i4\pi j/N_k}, \dots, e^{i2\pi j(N_k-1)/N_k}, 0, \dots, 0)}_{N_{k-1}^{\text{total}}} \quad : \quad \lambda_{k,j} = \epsilon^{2k}, \quad (41)$$

where $j = 1, 2, \dots, N_k - 1$. Thus, these modes are all located on the k th circle. For each $k = 2, 3, \dots, k_{\max}$, this set of $N_k - 1$ states is accompanied by a single slightly heavier mode with eigenvalue $\lambda_{k,N_k} \approx 2\epsilon^{2k}$, which approximately reads

$$\hat{H}_{\mu\nu}^{k,N_k} = \frac{1}{\sqrt{N_k^{\text{total}}}} \underbrace{(-1, \dots, -1, 1, \dots, 1, 0, \dots, 0)}_{N_{k-1}^{\text{total}}} \quad : \quad \lambda_{k,N_k} \approx 2\epsilon^{2k}. \quad (42)$$

Note, that to leading order these modes vanish outside the k th circle. As in Sec. 5.3, these non-localized profiles and the flat zero mode $\hat{H}_{\mu\nu}^{0,0}$ in Eq. (38) are only an artifact from working in the rough, local flat space approximation. In Fig. 8, a numerical calculation shows that the original mass matrix in Eq. (34) in fact reproduces a zero mode that is, as expected from the RS model, localized on the UV brane. Also the slightly heavier modes in Eq. (42) become localized on a single circle.

mass/ m_*^2	# of modes	wavefunction
0	1	Eq. (38)
ϵ^2	1	Eq. (39)
$3\epsilon^2$	1	Eq. (40)
ϵ^{2k}	$N_k - 1$	Eq. (41)
$\approx 2\epsilon^{2k}$	1	Eq. (42)

Table 1: Mass spectrum and wave-function profiles for the gravitons to leading order, taking into account only radial links. Here, $N_k = 2^k$ and $k = 2, 3, \dots, k_{\max}$.

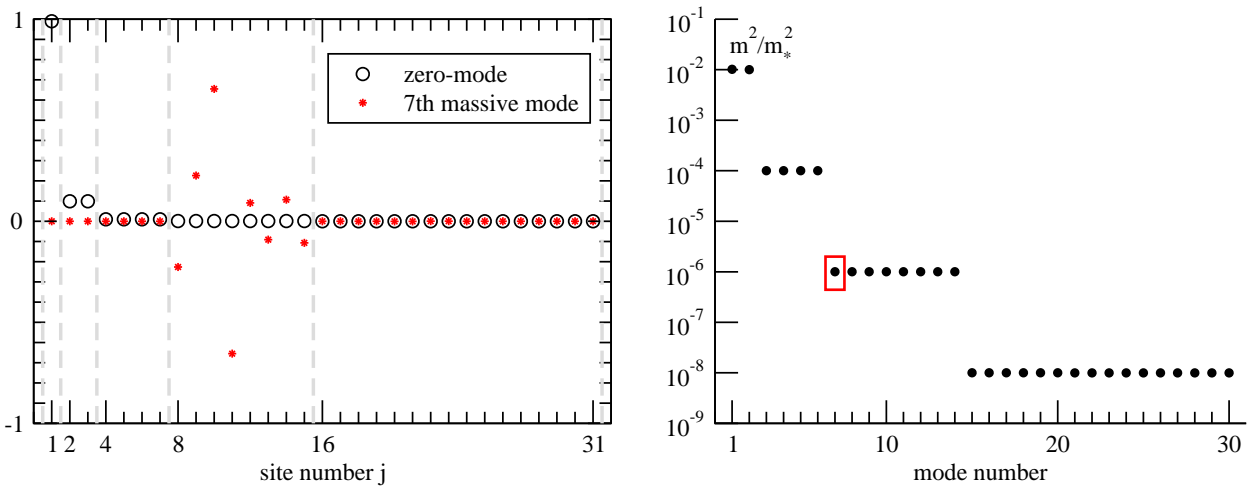


Figure 8: According to the “exact” mass matrix in Eq. (34), the left plot shows for $k_{\max} = 4$ and $\epsilon = 0.1$ the exact mode profiles of the zero mode (drawn as circles) and the 7th massive mode (drawn as stars). The latter would correspond to the mode in Eq. (42), when the rough local flat space approximation were used. The vertical dashed lines separate the sites on each circle, which illustrates that the zero mode is localized near the UV brane ($j = 1$) and that the 7th mode has support only on the third circle ($j = 8, \dots, 15$). The right plot shows the “exact” mass spectrum, where the 7th massive mode has been marked by a red box and the zero mode was omitted.

5.5 Effect of angular links

We can include the effect of the angular links on the total graviton mass matrix in Sec. 5.4 by adding to each sub-block spanned by the fields on the k th circle a matrix of the form

$$M_{ij}^k = m_k^2 (2\delta_{ij} - \delta_{i-1,j} - \delta_{i+1,j}), \quad (43)$$

where $i, j = 1, 2, \dots, N_k$ and m_k is the proper inverse lattice spacing on the k th circle as defined in Sec. 5.1. The inclusion of angular links in the fine-grained model is therefore similar in effect to what happens in the example of the coarse-grained model in Sec. 3.1. Switching on the angular links leaves the zero mode unaffected, but changes the masses of the degenerate modes $H_{\mu\nu}^{k,j}$ in Eq. (41) as

$$m_*^2 \epsilon^{2(k-1)} \lambda_{k,j} \rightarrow m_*^2 \epsilon^{2(k-1)} \epsilon^{2k} + 4m_k^2 \sin^2 \frac{j\pi}{N}, \quad (44)$$

where $j = 1, 2, \dots, N_k$. This is the analog of Eq. (15).

5.6 Local strong coupling scale

Let us now consider the local strong coupling scale on the discretized hyperbolic disk. By the same arguments as in Sec. 4.3, we will restrict ourselves here again to the case where only the effect of the radial links is taken into account and the interactions associated with the angular links can be neglected in the large N_k limit. To analyze the effective theory, we will use a new notation for the link fields that is different from the labelling employed previously in Secs. 3.1 and 4. From now on, in the notation of Sec. 5.4, a radial link field connecting two sites $(k-1, i)$ and (k, j) on two adjacent circles labelled by $k-1$ and k , where $k = 1, 2, \dots, N_k$, will be denoted by $Y_{k,j}^\mu(x_\mu)$. In analogy with Eq. (17b), we then expand this link field in the new notation as $Y_{k,j}^\mu = x^\mu + A_{kj}^\mu(x_\mu) + \partial^\mu \phi_{kj}(x_\mu)$. From Eq. (33), we then find for the total action

$$\begin{aligned} \mathcal{S}_{\text{lin}} = & \mathcal{S}_{\text{FP}} + \int d^4x M_4^2 \left[h_{\mu\nu}^{0,0} \square h_{\mu\nu}^{0,0} + \sum_{k=1}^{k_{\max}} \sum_{i=1}^{N_{k-1}} \left(\epsilon^{2k} h_{\mu\nu}^{k,i} \square h_{\mu\nu}^{k,i} + m_*^2 \epsilon^{4k} (h_{\mu\nu}^{k-1,i} - h_{\mu\nu}^{k,n_i}) \square \phi_{k,n_i} \right. \right. \\ & \left. \left. + m_*^2 \epsilon^{4k} (h_{\mu\nu}^{k-1,i} - h_{\mu\nu}^{k,n_i+1}) \square \phi_{k,n_i+1} + m_*^2 \epsilon^{4k} [(\square \phi_{k,n_i})^3 + (\square \phi_{k,n_i+1})^3] \right) \right], \end{aligned} \quad (45)$$

where $n_i = 2(i-1) + 1$. In the basis of canonically normalized fields $\hat{h}_{\mu\nu}^{k,i} = M_4 \epsilon^k h_{\mu\nu}^{k,i}$, the action \mathcal{S}_{lin} then reads

$$\begin{aligned} \mathcal{S}_{\text{lin}} = & \mathcal{S}_{\text{FP}} + \int d^4x \left[\hat{h}_{\mu\nu}^{0,0} \square \hat{h}_{\mu\nu}^{0,0} + \sum_{k=1}^{k_{\max}} \sum_{i=1}^{N_{k-1}} \left(\hat{h}_{\mu\nu}^{k,i} \square \hat{h}_{\mu\nu}^{k,i} + m_*^2 \epsilon^{3k} (\epsilon \hat{h}_{\mu\nu}^{k-1,i} - \hat{h}_{\mu\nu}^{k,n_i}) \square \phi_{k,n_i} \right. \right. \\ & \left. \left. + M_4 m_*^2 \epsilon^{3k} (\epsilon \hat{h}_{\mu\nu}^{k-1,i} - \hat{h}_{\mu\nu}^{k,n_i+1}) \square \phi_{k,n_i+1} + M_4^2 m_*^2 \epsilon^{4k} [(\square \phi_{k,n_i})^3 + (\square \phi_{k,n_i+1})^3] \right) \right]. \end{aligned} \quad (46)$$

Like in the rough, local flat space approximation of Sec. 5.2, let us now set in Eq. (46) $\epsilon = 1$ but keep the higher powers ϵ^{3k} , since k can be large. Consider now the subgraph in Fig. 7 for

the case $k_{\max} = 2$. For this subgraph, the kinetic mixing terms in Eq. (45) can be organized in a kinetic matrix that is proportional to

$$\begin{pmatrix} -1 & -1 & 0 & 0 & 0 & 0 \\ 1 & 0 & -\epsilon^3 & -\epsilon^3 & 0 & 0 \\ 0 & 1 & 0 & 0 & -\epsilon^3 & -\epsilon^3 \\ 0 & 0 & \epsilon^3 & 0 & 0 & 0 \\ 0 & 0 & 0 & \epsilon^3 & 0 & 0 \\ 0 & 0 & 0 & 0 & \epsilon^3 & 0 \\ 0 & 0 & 0 & 0 & 0 & \epsilon^3 \end{pmatrix}, \quad (47)$$

where we can choose a labelling such that the the rows and columns of the kinetic matrix are spanned by $(\hat{h}_{\mu\nu}^{0,0}, \hat{h}_{\mu\nu}^{1,1}, \hat{h}_{\mu\nu}^{1,2}, \hat{h}_{\mu\nu}^{2,1}, \hat{h}_{\mu\nu}^{2,2}, \hat{h}_{\mu\nu}^{2,3}, \hat{h}_{\mu\nu}^{2,4})$ and $(\phi_{1,1}, \phi_{1,2}, \phi_{2,1}, \phi_{2,2}, \phi_{2,3}, \phi_{2,4})$, respectively. Since the rank of the top-left 3×2 sub-matrix in Eq. (47) is 2, we see that the mixing between two scalar Goldstones $\phi_{k,i}$ and $\phi_{l,j}$ is small and only of order $\sim \epsilon^3$ for $k \neq l$, *i.e.*, the Goldstones associated with different concentric circles mix only little with each other. Let us expand the Goldstones as $\phi_{1,i} = \frac{1}{\sqrt{2}} \sum_{n=1}^2 e^{i2\pi i \cdot n/2} \Phi_{1,n}$, for $i = 1, 2$, and $\phi_{2,i} = \frac{1}{\sqrt{2}} \sum_{n=1}^2 e^{i2\pi i \cdot n/4} \Phi_{2,n}$, for $i = 1, 2, 3, 4$. Rotating to the basis of graviton mass eigenstates $(\hat{H}_{\mu\nu}^{0,0}, \hat{H}_{\mu\nu}^{1,1}, \hat{H}_{\mu\nu}^{1,2}, \hat{H}_{\mu\nu}^{2,1}, \hat{H}_{\mu\nu}^{2,2}, \hat{H}_{\mu\nu}^{2,3}, \hat{H}_{\mu\nu}^{2,4})$ as given in Eqs. (37), and going to the basis of Goldstones $(\Phi_{1,1}, \Phi_{1,2}, \Phi_{2,1}, \Phi_{2,2}, \Phi_{2,3}, \Phi_{2,4})$, the kinetic matrix in Eq. (47) becomes

$$\begin{pmatrix} 0 & 0 & 0 & 0 & 0 & 0 \\ 1 & 0 & e^{i\pi/4}\epsilon^3 & 0 & e^{-i\pi/4}\epsilon^3 & 0 \\ 0 & \sqrt{3} & 0 & 0 & 0 & -\sqrt{\frac{2}{3}}\epsilon^3 \\ 0 & 0 & \epsilon^3 & 0 & 0 & 0 \\ 0 & 0 & 0 & \epsilon^3 & 0 & 0 \\ 0 & 0 & 0 & 0 & \epsilon^3 & 0 \\ 0 & 0 & 0 & 0 & 0 & \sqrt{\frac{7}{3}}\epsilon^3 \end{pmatrix}, \quad (48)$$

which is, up to corrections of the order $\sim \epsilon^3$, on diagonal form. In a similar way, for general $k_{\max} \geq 2$, the kinetic mixing terms in Eq. (45) are approximately diagonalized by transforming to the graviton mass eigenbasis spanned by the fields $\hat{H}_{\mu\nu}^{k,j}$, as defined in Sec. 5.4, and by expanding the scalar Goldstones as $\phi_{k,i} = \frac{1}{\sqrt{N_k}} \sum_{n=1}^{N_k} e^{i2\pi i \cdot n/N_k} \Phi_{k,n}$, where $k = 1, 2, \dots, k_{\max}$ and $i = 1, 2, \dots, N_k$. In this basis, the action in Eq. (46) is then approximately

$$\begin{aligned} \mathcal{S}_{\text{ref}} = & \mathcal{S}_{\text{FP}} + \int d^4x \left[\hat{H}_{\mu\nu}^{0,0} \square \hat{H}_{\mu\nu}^{0,0} + \sum_{k=1}^{k_{\max}} \sum_{n=1}^{N_k} \left(\hat{H}_{\mu\nu}^{k,n} \square \hat{H}_{\mu\nu}^{k,-n} \right. \right. \\ & \left. \left. + M_4 m_*^2 \epsilon^{3k} \hat{H}_{\mu\nu}^{k,n} \square \Phi_{k,-n} + \sum_{m=1}^{N_k} M_4^2 \frac{m_*^2 \epsilon^{4k}}{\sqrt{N_k}} (\square \Phi_{k,n})(\square \Phi_{k,m})(\square \Phi_{k,-n-m}) \right) \right], \end{aligned} \quad (49)$$

where we have used the definitions $\hat{H}_{\mu\nu}^{k,-n} = \hat{H}_{\mu\nu}^{k,N_k-n}$ and $\Phi_{k,-n} = \Phi_{k,N_k-n}$. From Eq. (49), we read off the canonically normalized fields $\hat{\Phi}_{k,n} = M_4 m_*^2 \epsilon^{3k} \Phi_{k,n}$. In canonical normalization,

the tri-linear derivative coupling terms in Eq. (49) become

$$M_4 \frac{m_*^2 \epsilon^{4k}}{\sqrt{N_k}} (\square \Phi_{k,n})(\square \Phi_{k,m})(\square \Phi_{k,-n-m}) \rightarrow \frac{1}{\sqrt{N_k} M_k m_*^4 \epsilon^{4k}} (\square \hat{\Phi}_{k,n})(\square \hat{\Phi}_{k,m})(\square \hat{\Phi}_{k,-n-m}), \quad (50)$$

where $M_k = M_4 \epsilon^k$. Similar to Sec. 4, we then find that the modes $\hat{\Phi}_{k,n}$ in Eq. (50) become strongly coupled at a scale

$$\Lambda_k^{6D} = (\sqrt{N_k} M_k m_*^4 \epsilon^{4k})^{1/5}. \quad (51)$$

The important point is here the presence of the factor N_k , which can render the modes $\hat{\Phi}_{k,n}$ more weakly coupled for values $k \gtrsim 10$, where N_k becomes exponentially large. Such a factor N_k is absent in 5D lattice gravity models, *i.e.*, the presence of N_k in Eq. (51) is a benefit of working in a 6D setup. Setting, *e.g.*, the inverse radial lattice spacing $m_* = M_4$, it follows that $\Lambda_k^{6D} = N_k^{1/10} M_k$, which would be a factor $N_k^{1/10}$ above the local Planck scale M_k . But having Λ_k^{6D} significantly above M_k , requires many sites N_k on the k th circle. In our special example, with $\ell = 2$ and $k_{\max} \simeq 15$, we have $N_{k_{\max}}^{1/10} \approx 3$. For $\ell \simeq 5$, however, we obtain $N_{k_{\max}}^{1/10} \simeq 10$, while keeping $\epsilon \cdot \ell \simeq 0.5$ sufficiently small.

The scale Λ_k^{6D} in Eq. (51), has been found by first going in Eq. (46) to the rough, local flat space approximation and then neglecting the mixing between modes on neighboring circles. We will now, however, be interested in taking the nonzero mixing effects between the modes on neighboring circles into account. In doing so, we will follow closely the argumentation presented for the warped 5D case in Ref. [12]. Like in the 5D case, the modes which are relevant for the strong coupling scale at some site, have a maximum wavelength in radial direction which is of the order the inverse curvature scale $1/w$, and it is these long-wavelength modes, which become most earliest strongly coupled. Considering within distances $\sim 1/w$ in radial direction the space as locally flat and treating the modes in this regime as plane waves, it is seen in our calculation that the mixing of the modes between neighboring circles can be approximately taken into account by sending in Eq. (51) $m_*^4 \epsilon^{4k} \rightarrow (w/M_4)^3 m_*^4 \epsilon^{4k}$ and $N_k \rightarrow (M_4/w) N_k$. We thus obtain from Eq. (51) a local strong coupling scale at the k th circle that is approximately

$$\Lambda_{\text{warp}}^{6D} = \sqrt{\frac{w}{M_4}} (\sqrt{N_k} M_k m_*^4 \epsilon^{4k})^{1/5}. \quad (52)$$

With respect to Λ_k^{6D} in Eq. (51), the local strong coupling scale $\Lambda_{\text{warp}}^{6D}$ is lowered by a factor $(w/M_4)^{1/2}$, which is for our choice of parameters (see Sec. 5.2) of the order $(w/M_4)^{1/2} \approx 0.3$. Setting in Eq. (52) $m_* = M_4$, one arrives at $\Lambda_{\text{warp}}^{6D} = (w/M_4)^{1/2} N_k^{1/10} M_k$. In our example with $\ell = 2$, the local strong coupling scale will therefore be pushed to values higher than the local Planck scale M_k , for $k \gtrsim 15$. For $\ell = 3$, this happens already for $k \gtrsim 10$. Note also, that $\Lambda_{\text{warp}}^{6D}$ reproduces in the limit $N_k \rightarrow 1$ the local strong coupling scale in 5D warped space as determined in Ref. [12].

It is instructive to compare $\Lambda_{\text{warp}}^{6D}$ with the strong coupling scales in 5D lattice gravity. In 5D flat space, the strong coupling scale is $\Lambda_{\text{flat}}^{5D} = (N^{3/2} M_4 m_1^4)^{1/5}$, where m_1 is the mass of the lightest graviton and N is the number of lattice sites [7]. Since $m_1 = m/N$, where m is the inverse lattice spacing, we see that even for m as large as M_4 , the strong coupling

scale $\Lambda_{\text{flat}}^{5D}$ is always smaller than the local Planck scale M_4 , and $\Lambda_{\text{flat}}^{5D}$ goes to zero in the large volume limit $N \rightarrow \infty$. This situation is remedied in 5D warped space, where the local strong coupling scale is $\Lambda_{\text{warp}}^{5D} = (w/M_4)^{1/2}M_k$, in which w is the 5D curvature scale and $M_k = M_4 e^{-kw/m}$ is the local Planck scale at the k th site [12]. The strong coupling scale $\Lambda_{\text{warp}}^{5D}$ is independent from N , which allows to take the large volume limit like in RS II [2]. However, $\Lambda_{\text{warp}}^{5D}$ is still smaller by a factor $(w/M_4)^{1/2}$ than M_k . On our warped hyperbolic disk, on the other hand, $\Lambda_{\text{warp}}^{6D}$ is (i) independent from the number of concentric circles k_{max} and can (ii) be as large as as the local Planck scale M_k , when approaching the boundary.

6 Application to Dirac neutrino masses

So far, we have only been considering the case where gravity is propagating on the disk. In this section, we will be concerned with matter in the bulk and formulate a model for small Dirac neutrino masses by implementing on the hyperbolic disk a discretized version of the volume suppression mechanism of Ref. [28]. For simplicity, we shall restrict here to the coarse-grained model described in Sec. 3. The parent continuum theory, which we discretize, contains a massless right-handed (RH), *i.e.*, SM singlet, bulk neutrino that can propagate on the disk or some sub-space thereof, while the SM fields are all located on a single point of the disk. Specifically, we consider the total action of the bulk neutrino on the disk as a combination of the following two limiting cases: (i) the bulk neutrino propagates only within the star sub-geometry of the disk and (ii) the bulk neutrino propagates only in the circle sub-geometry.

Let us first consider case (i): the action for the gravitons is described by $\mathcal{S}_{\text{disk}}$ in Sec. 4.3, but the latticized RH bulk neutrino propagates only in the star sub-geometry. The bulk neutrino is represented in the discretized theory by putting on each site i one 4D RH SM singlet Dirac fermion $\Psi_i = (\nu_{Ri}, \overline{\nu}_{Ri}^c)$, where ν_{Ri} and $\overline{\nu}_{Ri}^c$ are 4D two-component Weyl spinors and $i = 0, 1, \dots, N$. The star sub-geometry, with N sites surrounding the center, can be thought as being composed of N two-site models that are glued together at the site $i = 0$. It is convenient to label these two-site models as $(0, i)$, where $i = 1, 2, \dots, N$. To obtain here the action of the right-handed bulk neutrino, we consider each two-site model $(0, i)$ as the coarse-grained limit of a latticized fifth dimension that is compactified on an interval $[0, R_i]$ and apply discretized orbifold boundary conditions at the endpoints. In this picture, the continuum limit of the star sub-geometry is a configuration of N continuous intervals $[0, R_i]$, which intersect in their common endpoint 0. The RH bulk neutrino propagates in this continuum theory as a 5D field on the intervals and is subject to orbifold boundary conditions at the endpoints of the segments $[0, R_i]$. We denote the 5D bulk neutrino by $\Psi = (\nu_R, \overline{\nu}_R^c)$, where ν_R and $\overline{\nu}_R^c$ are 5D two-component Weyl spinors, and assume on each of the N intervals the Neumann and Dirichlet boundary conditions $(\partial \nu_R / \partial y_i)|_{y_i=0, R_i} = 0$ and $\nu_R^c|_{y_i=0, R_i} = 0$, where $y_i \in [0, R_i]$ is the coordinate of the interval $[0, R_i]$ and $i = 1, 2, \dots, N$. The discretization of these boundary conditions has been described in Refs. [11, 15, 29] and produces, in the limit where each interval $[0, R_i]$ is replaced by a two-site model $(0, i)$, from the latticized kinetic term of Ψ the neutrino mass terms

$$\mathcal{L}_{(0,i)} = m_* (\nu_{iR} \nu_{iR}^c - \nu_{0R} \nu_{0R}^c) + \text{h.c.}, \quad (53)$$

where we have chosen a common length $R_i \equiv R \sim m_*^{-1}$ for all intervals. In the flat limit $g_{\mu\nu} \rightarrow \eta_{\mu\nu}$, we then take the total action for the bulk neutrino in the star sub-geometry $\mathcal{S}_{\text{star}}^\Psi$ to be $\mathcal{S}_{\text{star}}^\Psi = \int d^4x (\sum_{i=0}^N i \bar{\Psi}_i \not{\partial} \Psi_i + \sum_{i=1}^N \mathcal{L}_{(0,i)})$. To include the effect from the boundary, let us next consider case (ii): the latticized bulk RH neutrino propagates only on the boundary of the disk. For this case, we take the action of the latticized RH neutrino on the circle $\mathcal{S}_{\text{circle}}^\Psi$ to be of the Wilson-Dirac form $\mathcal{S}_{\text{circle}}^\Psi = \int d^4x \sum_{i=1}^N (i \bar{\Psi}_i \not{\partial} \Psi_i + \mathcal{L}_{(i,i+1)})$, where we have introduced a discretized kinetic term

$$\mathcal{L}_{(i,i+1)} = m \cdot \nu_{iR} (\nu_{(i+1)R}^c - \nu_{iR}^c) + \text{h.c.}, \quad (54)$$

for each pair of sites $(i, i+1)$ on the boundary of the disk. For definiteness, we suppose also that N is even. The action $\mathcal{S}_{\text{circle}}^\Psi$ has been widely discussed in the literature as a standard example for a fermion propagating in a latticized fifth dimension compactified on the circle S^1 [11] (see also, *e.g.*, Refs. [21, 22]). Now, we define the total action of the bulk neutrino on the disk $\mathcal{S}_{\text{disk}}^\Psi$ by simply adding the mass terms $\mathcal{L}_{(i,i+1)}$ to $\mathcal{S}_{\text{star}}^\Psi$ such that

$$\mathcal{S}_{\text{disk}}^\Psi = \int d^4x \left(\sum_{i=0}^N i \bar{\Psi}_i \not{\partial} \Psi_i + \sum_{i=1}^N [\mathcal{L}_{(0,i)} + C \cdot \mathcal{L}_{(i,i+1)}] \right), \quad (55)$$

where C is some suitable dimensionless parameter. The mass terms in Eq. (55) give rise to the Dirac neutrino mass matrix

$$M_D = m_* \begin{pmatrix} 0 & -1 & -1 & \cdots & -1 \\ 0 & 1 & 0 & \cdots & 0 \\ 0 & 0 & 1 & \ddots & \vdots \\ \vdots & \vdots & \ddots & \ddots & 0 \\ 0 & 0 & \cdots & 0 & 1 \end{pmatrix} - Cm \begin{pmatrix} -1 & 1 & 0 & \cdots & 0 \\ 0 & -1 & 1 & \ddots & \vdots \\ \vdots & 0 & \ddots & \ddots & 0 \\ 0 & \vdots & \ddots & -1 & 1 \\ 1 & 0 & \cdots & 0 & -1 \end{pmatrix}, \quad (56)$$

where the rows and columns are spanned by $(\nu_{R1}, \nu_{R2}, \dots, \nu_{RN})$ and $(\nu_{R1}^c, \nu_{R2}^c, \dots, \nu_{RN}^c)$, respectively. We can choose the parameter C such that the matrix $M_D M_D^\dagger$ becomes identical with the graviton mass matrix M_g^2 in Eq. (14) and the right-handed neutrino masses are given by Eq. (15). The mass matrix in Eq. (56) is then diagonalized by expanding

$$\nu_{0R} = \frac{1}{\sqrt{N+1}} \hat{\nu}_{0R} - \frac{N}{\sqrt{N(N+1)}} \hat{\nu}_{NR}, \quad (57a)$$

$$\nu_{iR} = \frac{1}{\sqrt{N}} \sum_{n=1}^{N-1} e^{-i2\pi i \cdot n/N} \hat{\nu}_{nR} + \frac{1}{\sqrt{N+1}} \hat{\nu}_{0R} + \frac{1}{\sqrt{N(N+1)}} \hat{\nu}_{NR}, \quad (57b)$$

where $i = 1, 2, \dots, N$ and $\hat{\nu}_{nR}$ ($n = 0, 1, \dots, N$) is the n th mass eigenstate belonging to the mass eigenvalue M_n^2 given in Eq. (15). In Eq. (57) we thus have one zero mode neutrino $\hat{\nu}_{0R}$ with flat profile, one heavy neutrino $\hat{\nu}_{NR}$ with mass $M_N \sim m_* \sqrt{N}$ and $N-1$ states $\hat{\nu}_{1R}, \hat{\nu}_{2R}, \dots, \hat{\nu}_{N-1}$ with masses M_n , where $M_n \approx m_*$ for $m_* \gg m$.

Let us now introduce the SM neutrinos by adding all SM fields on a single site on the boundary, *e.g.*, on the site $i = 1$. To simplify the discussion, we assume like in Ref. [28] that

$B - L$ is conserved in the bulk and assign to the bulk neutrino a $B - L$ number opposite to that of the SM leptons. On the site $i = 1$, we then have a local Yukawa interaction $\mathcal{L}_{\text{int}} = f_\alpha \ell_\alpha i\sigma_2 H \nu_{1R}$, where $\ell_\alpha = (\nu_\alpha, e_\alpha)^T$ are the lepton doublets with generation index $\alpha = 1, 2, 3$, H is the Higgs doublet, and f_α a dimensionless order one Yukawa coupling. Going to momentum basis, \mathcal{L}_{int} approximately reads

$$\mathcal{L}_{\text{int}} \approx f_\alpha \frac{\langle H \rangle}{\sqrt{N}} \nu_\alpha \hat{\nu}_{0R}, \quad (58)$$

and produces a Dirac neutrino mass term between the active neutrinos ν_α and $\hat{\nu}_{0R}$, that is suppressed by a volume factor $\sqrt{N} = \sqrt{Rm}$. This is the analog of the volume suppression mechanism in Ref. [28]. In the coarse-grained model, for $m_* \sim m$, and $x \equiv v/m_* \gtrsim 1$, we have $N \simeq \pi \exp(x - \ln x)$, *i.e.*, a moderately large curvature v (*e.g.*, $v/m_* = \mathcal{O}(10)$), gives an exponentially large number of sites N . For $\langle H \rangle \simeq 10^2$ GeV and $N \simeq 10^{24}$ sites, the Dirac neutrino masses will be of the right order 10^{-2} eV, which would correspond to $v/m_* \simeq 60$ in the above approximation. The important point is here, that the strong coupling scale does in the coarse-grained model not drop below $\Lambda_{\text{disk}} = (M_{\text{Pl}} m_*^4)^{1/5}$ in the large N (or large volume) limit. Since all massive neutrino singlets have a mass larger than m_* , it follows that for $m_* \gtrsim 1$ GeV, all constraints on KK neutrinos from astrophysics and the early universe [30] are avoided.

7 Summary and Conclusions

In this paper, we have investigated gravity in a 6D geometry, where the two extra dimensions are discretized and form a hyperbolic disk with constant curvature. We have studied two types of discretizations of the disk. In our first model, we have considered a coarse-grained discretization with a number of N sites on the boundary and one site in the center of the disk. For this case, we have determined the mass spectrum and mass eigenstates of the gravitons and found in the limit of large curvature a typical KK-type of spectrum sitting on top of a large mass gap between the zero mode and the first massive mode. This mass gap is set by the inverse radius of the disk while the other modes become essentially degenerate in mass. This feature allows to avoid all existing constraints on KK gravitons from Cavendish-type experiments, astrophysics and cosmology. Additionally, this model contains a single massive mode, which becomes very heavy in the large N limit. We have also discussed some collider signatures of this coarse-grained model at the LHC and a possible future linear collider.

The strong coupling scale in this coarse-grained model converges for large N to a value like in the theory of a single massive graviton, where the graviton has a mass of the order the inverse proper radius of the disk. This is completely different from a discrete gravitational extra dimension in 5D flat space, which exhibits a UV/IR connection problem, where the strong coupling scale would eventually go to zero when taking the large N limit. This UV/IR connection problem, however, is absent in the coarse-grained model, where a sensible EFT is defined in the large N limit. In this model, we have also studied an implementation of a bulk fermion, which allows to generate small Dirac neutrino masses in the limit of a large curvature of the disk via a discrete version of the well-known volume suppression mechanism

for Dirac neutrino masses in flat extra dimensions. Again, due to the particular form of the spectrum, all experimental and observational constraints on the massive KK-type neutrinos are avoided.

In our second model, we describe a fine-grained discretization of the hyperbolic disk with nonzero warping along the radial direction. In this setup, the sites are situated on equidistant concentric circles and, as a result of the curvature of the disk, the number of sites on the circles grows exponentially in radial direction. We have calculated the graviton mass eigenvalues and mass eigenstates in the fine-grained model by going, as suggested previously in an analysis of the discretized 5D RS model, to a rough, local flat space approximation. Moreover, we have determined in the fine-grained model a local strong coupling scale from the kinetic mixing matrix between the gravitons and scalar Goldstones. The existence of a local strong coupling scale in the fine-grained model is, like in the corresponding 5D case, a result of the warping, which avoids the UV/IR connection problem from flat space by locally introducing an effective size or volume of the extra dimensions. In the fine-grained model, the local strong coupling scale at some site depends on the radial coordinate and is a function of the total number of sites on the concentric circle through this site. It turns out that, for an exponentially large number of sites on the circle, the local strong coupling scale is shifted to values that are higher than in the corresponding 5D warped case. A sufficiently large number of sites is provided on the hyperbolic disk, when approaching the IR branes on the boundary. As a consequence, the local strong coupling scale can be as high as the local Planck scale on the IR branes, which is an improvement with respect to the strong coupling behavior of discretized gravity in the 5D warped case.

In conclusion, we have seen for different implementations of two discrete gravitational extra dimensions compactified on a hyperbolic disk, that a high curvature or strong warping of the disk allows to avoid the UV/IR connection problem of lattice gravity in flat space. This observation is similar to the result in 5D warped case. By going to six dimensions on the hyperbolic disk, however, it is possible to improve further on the strong coupling behavior of the 5D warped case and achieve on the IR branes a description of lattice gravity that is valid up to the local Planck scale. Moreover, a strong curvature of the disk allows to avoid all constraints on KK-states and can, *e.g.*, be employed for generating small Dirac neutrino masses in agreement with experiment.

It would be interesting to relate our analysis, *e.g.*, also to moduli stabilization in effective theories, to theories with spontaneously broken space-time symmetries [31], and to studies on the implications of latticized extra dimensions for cosmology [32].

Acknowledgements

We would like to thank K.S. Babu, I. Bengtsson, M. Blennow, T. Konstandin, T. Ohlsson, and M.D. Schwartz for useful comments and discussions. This work was supported by the “Sonderforschungsbereich 375 für Astroteilchenphysik der Deutschen Forschungsgemeinschaft” (F.B.), the Göran Gustafsson Foundation (T.H.) and the U.S. Department of Energy under grant number DE-FG02-04ER46140 (G.S.).

A Gravitational action on the hyperbolic disk

In this section, we determine the gravitational action on the hyperbolic disk K_2 introduced in Sec. 2. We start with the 6D metric \tilde{g}_{MN} as defined in Eq. (1), where $\tilde{g}_{\mu\nu} = e^{2\sigma(r)}g_{\mu\nu}$, $\tilde{g}_{55} = -1$, and $\tilde{g}_{66} = -\sinh^2(vr)/(v^2)$. Partial and covariant derivatives are denoted by commas and semicolons, respectively. In these coordinates, the nonzero Christoffel symbols are

$$\begin{aligned}\Gamma_{\mu\nu}^\sigma &= \frac{1}{2}\tilde{g}^{\sigma\rho}(\tilde{g}_{\mu\rho,\nu} + \tilde{g}_{\rho\nu,\mu} - \tilde{g}_{\mu\nu,\rho}), \\ \Gamma_{\nu 5}^\mu &= \frac{1}{2}\tilde{g}^{\mu\rho}\tilde{g}_{\nu\rho,5}, \quad \Gamma_{\nu 6}^\mu = \frac{1}{2}\tilde{g}^{\mu\rho}\tilde{g}_{\nu\rho,6}, \quad \Gamma_{\mu\nu}^5 = -\frac{1}{2}\tilde{g}^{55}\tilde{g}_{\mu\nu,5}, \quad \Gamma_{\mu\nu}^6 = -\frac{1}{2}\tilde{g}^{66}\tilde{g}_{\mu\nu,6}, \\ \Gamma_{66}^5 &= -\frac{1}{2}\tilde{g}^{55}\tilde{g}_{66,5} = -\frac{1}{2v}\sinh(2vr), \quad \Gamma_{56}^6 = \frac{1}{2}\tilde{g}^{66}\tilde{g}_{66,5} = v\coth(vr),\end{aligned}\quad (59)$$

where $\Gamma_{BC}^A = \Gamma_{CB}^A$. Note, that due to the block-diagonal form of the metric \tilde{g}_{MN} , the internal summation in $\Gamma_{\mu\nu}^\sigma$ runs only over 4D indices. The 6D Ricci tensor is defined by $\tilde{R}_{MN} = \Gamma_{MA,N}^A - \Gamma_{MN,A}^A + \Gamma_{BN}^A\Gamma_{MA}^B - \Gamma_{MN}^B\Gamma_{BA}^A$ and the 6D Ricci scalar is $\tilde{R} = \tilde{R}_{MN}\tilde{g}^{MN}$. It is useful to introduce the quantity

$$\tilde{R}_{4D} = \tilde{g}^{\mu\nu}[\Gamma_{\mu\alpha,\nu}^\alpha - \Gamma_{\mu\nu,\alpha}^\alpha + \Gamma_{\beta\nu}^\alpha\Gamma_{\mu\alpha}^\beta - \Gamma_{\mu\nu}^\beta\Gamma_{\beta\alpha}^\alpha]. \quad (60)$$

Since the warp factor is only a function of r , we have $\Gamma_{\mu\nu}^\sigma = \frac{1}{2}\tilde{g}^{\sigma\rho}(g_{\mu\rho,\nu} + g_{\rho\nu,\mu} - g_{\mu\nu,\rho})$ and the 4D Ricci scalar R_{4D} in Eq. (7) is thus related to \tilde{R}_{4D} by $R_{4D} = e^{2\sigma(r)}\tilde{R}_{4D}$. In Eq. (6), we can write $\sqrt{|\tilde{g}|}\tilde{R} = \sqrt{|\tilde{g}|}(\tilde{g}^{\mu\nu}\tilde{R}_{\mu\nu} + \tilde{g}^{55}\tilde{R}_{55} + \tilde{g}^{66}\tilde{R}_{66})$, where the first term reads

$$\begin{aligned}\sqrt{|\tilde{g}|}\tilde{g}^{\mu\nu}\tilde{R}_{\mu\nu} &= \sqrt{|\tilde{g}|}\tilde{g}^{\mu\nu}[\Gamma_{\mu\alpha,\nu}^\alpha - \Gamma_{\mu\nu,\alpha}^\alpha + \Gamma_{\beta\nu}^\alpha\Gamma_{\mu\alpha}^\beta - \Gamma_{\mu\nu}^\beta\Gamma_{\beta\alpha}^\alpha \\ &\quad - \Gamma_{\mu\nu,5}^5 + \Gamma_{\beta\nu}^5\Gamma_{\mu 5}^\beta + \Gamma_{5\nu}^\alpha\Gamma_{\mu\alpha}^5 - \Gamma_{\mu\nu}^5\Gamma_{5A}^A - \Gamma_{\mu\nu,6}^6 + \Gamma_{\beta\nu}^6\Gamma_{\mu 6}^\beta + \Gamma_{6\nu}^\alpha\Gamma_{\mu\alpha}^6 - \Gamma_{\mu\nu}^6\Gamma_{6A}^A].\end{aligned}\quad (61)$$

Here, the derivative of the Christoffel symbol with respect to r (or φ) can be written as

$$-\sqrt{|\tilde{g}|}\tilde{g}^{\mu\nu}\Gamma_{\mu\nu,5}^5 = -\left[\sqrt{|\tilde{g}|}\tilde{g}^{\mu\nu}\Gamma_{\mu\nu}^5\right]_5 + \sqrt{|\tilde{g}|}\tilde{g}^{\mu\nu}\Gamma_{A5}^A\Gamma_{\mu\nu}^5 - 2\sqrt{|\tilde{g}|}\tilde{g}^{\mu\alpha}\Gamma_{\alpha 5}^\nu\Gamma_{\mu\nu}^5, \quad (62)$$

where we have used the identities $(\sqrt{|\tilde{g}|})_A = \sqrt{|\tilde{g}|}\Gamma_{BA}^A$ and $\tilde{g}^{\mu\nu,5} = -\tilde{g}^{\mu\alpha}\tilde{g}^{\nu\beta}\tilde{g}_{\alpha\beta,5} = -2\tilde{g}^{\mu\alpha}\Gamma_{\alpha 5}^\nu$ to obtain respectively the second and the third term on the right-hand side in Eq. (62). We thus have

$$\sqrt{|\tilde{g}|}\tilde{g}^{\mu\nu}\tilde{R}_{\mu\nu} = \sqrt{|\tilde{g}|}\tilde{R}_{4D} - \left[\sqrt{|\tilde{g}|}\tilde{g}^{\mu\nu}\Gamma_{\mu\nu}^5\right]_5 - \left[\sqrt{|\tilde{g}|}\tilde{g}^{\mu\nu}\Gamma_{\mu\nu}^6\right]_6, \quad (63)$$

Similarly, one finds

$$\begin{aligned}\sqrt{|\tilde{g}|}\tilde{g}^{55}\tilde{R}_{55} &= \left[\sqrt{|\tilde{g}|}\tilde{g}^{55}\Gamma_{A5}^A\right]_5 - \left[\sqrt{|\tilde{g}|}\tilde{g}^{55}\Gamma_{55}^A\right]_A \\ &\quad + \sqrt{|\tilde{g}|}\tilde{g}^{55}[\Gamma_{\beta 5}^\alpha\Gamma_{\alpha 5}^\beta - \Gamma_{\alpha 5}^\alpha\Gamma_{\beta 5}^\beta - 2\Gamma_{\alpha 5}^\alpha\Gamma_{65}^6],\end{aligned}\quad (64a)$$

$$\sqrt{|\tilde{g}|}\tilde{g}^{66}\tilde{R}_{66} = \left[\sqrt{|\tilde{g}|}\tilde{g}^{66}\Gamma_{A6}^A\right]_6 - \left[\sqrt{|\tilde{g}|}\tilde{g}^{66}\Gamma_{66}^A\right]_A + \sqrt{|\tilde{g}|}\tilde{g}^{66}[\Gamma_{\beta 6}^\alpha\Gamma_{\alpha 6}^\beta - \Gamma_{\alpha 6}^\alpha\Gamma_{\beta 6}^\beta]. \quad (64b)$$

In Eqs. (64), we have

$$\begin{aligned} & \sum_{B=5,6} \left(\left[\sqrt{|\tilde{g}|} \tilde{g}^{BB} \Gamma_{AB}^A \right]_{,B} - \left[\sqrt{|\tilde{g}|} \tilde{g}^{BB} \Gamma_{BB}^A \right]_{,A} - \left[\sqrt{|\tilde{g}|} \tilde{g}^{\mu\nu} \Gamma_{\mu\nu}^B \right]_{,B} \right) \\ &= \left[\sqrt{|\tilde{g}|} (-\tilde{g}^{\mu\nu} \Gamma_{\mu\nu}^6 + \tilde{g}^{66} \Gamma_{\alpha 6}^\alpha) \right]_{,6} + \left[\sqrt{|\tilde{g}|} (-\tilde{g}^{\mu\nu} \Gamma_{\mu\nu}^5 + \tilde{g}^{55} \Gamma_{\alpha 5}^\alpha - \tilde{g}^{66} \Gamma_{66}^5 + \tilde{g}^{55} \Gamma_{65}^6) \right]_{,5}, \end{aligned} \quad (65)$$

and in Eq. (65) the last two terms can be written as

$$\left[\sqrt{|\tilde{g}|} (-\tilde{g}^{66} \Gamma_{66}^5 + \tilde{g}^{55} \Gamma_{65}^6) \right]_{,5} = 2\sqrt{|\tilde{g}|} \tilde{g}^{55} \Gamma_{\alpha 5}^\alpha \Gamma_{65}^6 + 2\sqrt{|\tilde{g}|} \tilde{g}^{55} ((\Gamma_{65}^6)^2 + \Gamma_{65,5}^6), \quad (66)$$

where we have used the relation $\tilde{g}^{66} \Gamma_{66}^5 = -\tilde{g}^{55} \Gamma_{65}^6$. The first term on the right-hand side in Eq. (66) cancels the term $-2\sqrt{|\tilde{g}|} \tilde{g}^{55} \Gamma_{\alpha 5}^\alpha \Gamma_{65}^6$ in Eq. (64a), while the last term yields the cosmological term $\sqrt{|\tilde{g}|} \cdot (-2v^2)$. Putting everything together, the total action \mathcal{S} in Eq. (6) can be written as $\mathcal{S} = \mathcal{S}_{4D} + \mathcal{S}_{\text{surface}} + \mathcal{S}_{\text{mass}}$, where \mathcal{S}_{4D} , the surface terms $\mathcal{S}_{\text{surface}}$ and the action $\mathcal{S}_{\text{mass}}$, giving rise to the graviton mass terms, respectively read

$$\mathcal{S}_{4D} = M_6^4 \int d^6x \sqrt{|\tilde{g}|} (\tilde{R}_{4D} - 2v^2), \quad (67a)$$

$$\mathcal{S}_{\text{surface}} = M_6^4 \int d^6x \left(2 \left[\sqrt{|\tilde{g}|} \tilde{g}^{55} \Gamma_{\alpha 5}^\alpha \right]_{,5} + 2 \left[\sqrt{|\tilde{g}|} \tilde{g}^{66} \Gamma_{\alpha 6}^\alpha \right]_{,6} \right), \quad (67b)$$

$$\mathcal{S}_{\text{mass}} = M_6^4 \int d^6x \sqrt{|\tilde{g}|} \left(\tilde{g}^{55} [\Gamma_{\beta 5}^\alpha \Gamma_{\alpha 5}^\beta - \Gamma_{\alpha 5}^\alpha \Gamma_{\beta 5}^\beta] + \tilde{g}^{66} [\Gamma_{\beta 6}^\alpha \Gamma_{\alpha 6}^\beta - \Gamma_{\alpha 6}^\alpha \Gamma_{\beta 6}^\beta] \right). \quad (67c)$$

Let us first consider $\mathcal{S}_{\text{surface}}$, which reads

$$\mathcal{S}_{\text{surface}} = M_6^4 \int d^4x \int_0^{2\pi} d\varphi \int_0^L dr \left(\left[\sqrt{|\tilde{g}|} \tilde{g}^{55} \tilde{g}^{\mu\nu} \tilde{g}_{\mu\nu,5} \right]_{,5} + \left[\sqrt{|\tilde{g}|} \tilde{g}^{66} \tilde{g}^{\mu\nu} \tilde{g}_{\mu\nu,6} \right]_{,6} \right).$$

The φ -integral over the second term vanishes for periodic boundary conditions in φ -direction and the first term yields $\mathcal{S}_{\text{surface}} = M_6^4 \int d^4x \int_0^{2\pi} d\varphi [\sqrt{|\tilde{g}|} \tilde{g}^{55} \tilde{g}^{\mu\nu} \tilde{g}_{\mu\nu,5}]_{r=0}^{r=L}$, which vanishes for suitable boundary conditions at $r = 0, L$. In a simplified form, $\mathcal{S}_{\text{mass}}$ can be written as

$$\mathcal{S}_{\text{mass}} = M_6^4 \int d^6x \sqrt{|\tilde{g}|} \sum_{c=5,6} \left[-\frac{1}{4} \tilde{g}^{cc} \tilde{g}_{\mu\nu,c} (\tilde{g}^{\mu\nu} \tilde{g}^{\alpha\beta} - \tilde{g}^{\mu\alpha} \tilde{g}^{\nu\beta}) \tilde{g}_{\alpha\beta,c} \right]. \quad (68)$$

With $\tilde{g}_{\mu\nu} = e^{2\sigma(r)} g_{\mu\nu}$, $|\tilde{g}| = e^{8\sigma(r)} |g|$, and $R_{4D} = e^{2\sigma(r)} \tilde{R}_{4D}$, we then arrive at Eq. (7).

References

- [1] L. Randall and R. Sundrum, Phys. Rev. Lett. **83** (1999) 3370, [hep-ph/9905221](#).
- [2] L. Randall and R. Sundrum, Phys. Rev. Lett. **83** (1999) 4690, [hep-th/9906064](#).
- [3] N. Arkani-Hamed, S. Dimopoulos, and G.R. Dvali, Phys. Lett. B **429** (1998) 263, [hep-ph/9803315](#); Phys. Rev. D **59** (1999) 086004, [hep-ph/9807344](#); I. Antoniadis, N. Arkani-Hamed, S. Dimopoulos, and G.R. Dvali, Phys. Lett. B **436** (1998) 257, [hep-ph/9804398](#).

- [4] J.M. Maldacena, *Adv. Theor. Math. Phys.* **2** (1998) 231 [*Int. J. Theor. Phys.* **38** (1999) 1113], [hep-th/9711200](#); S.S. Gubser, I.R. Klebanov, and A.M. Polyakov, *Phys. Lett. B* **428** (1998) 105, [hep-th/9802109](#); E. Witten, *Adv. Theor. Math. Phys.* **2** (1998) 253, [hep-th/9802150](#); O. Aharony, S.S. Gubser, J.M. Maldacena, H. Ooguri, and Y. Oz, *Phys. Rept.* **323** (2000) 183, [hep-th/9905111](#).
- [5] See, *e.g.*, S.B. Giddings, S. Kachru, and J. Polchinski, *Phys. Rev. D* **66** (2002) 106006, [hep-th/0105097](#), and references therein.
- [6] N. Arkani-Hamed, H. Georgi, and M.D. Schwartz, *Annals Phys.* **305** (2003) 96, [hep-th/0210184](#).
- [7] N. Arkani-Hamed and M.D. Schwartz, *Phys. Rev. D* **69** (2004) 104001, [hep-th/0302110](#).
- [8] M.D. Schwartz, *Phys. Rev. D* **68** (2003) 024029, [hep-th/0303114](#).
- [9] N. Boulanger, T. Damour, L. Gualtieri and M. Henneaux, *Nucl. Phys. B* **597** (2001) 127, [hep-th/0007220](#); T. Damour, I.I. Kogan and A. Papazoglou, *Phys. Rev. D* **66** (2002) 104025, [hep-th/0206044](#); C. Deffayet and J. Mourad, *Class. Quant. Grav.* **21** (2004) 1833, [hep-th/0311125](#); G. Cognola, E. Elizalde, S. Nojiri, S. D. Odintsov and S. Zerbini, *Mod. Phys. Lett. A* **19** (2004) 1435, [hep-th/0312269](#).
- [10] N. Arkani-Hamed, A.G. Cohen, and H. Georgi, *Phys. Rev. Lett.* **86** (2001) 4757, [hep-th/0104005](#).
- [11] C.T. Hill, S. Pokorski, and J. Wang, *Phys. Rev. D* **64** (2001) 105005, [hep-th/0104035](#).
- [12] L. Randall, M.D. Schwartz, and S. Thambyapillai, *JHEP* **0510** (2005) 110, [hep-th/0507102](#).
- [13] J. Gallicchio and I. Yavin, [hep-th/0507105](#).
- [14] A. Falkowski and H.D. Kim, *JHEP* **0208** (2002) 052, [hep-ph/0208058](#).
- [15] T. Bhattacharya, C. Csaki, M.R. Martin, Y. Shirman, and J. Terning, *JHEP* **0508** (2005) 061, [hep-lat/0503011](#).
- [16] H.C. Cheng, C.T. Hill, and J. Wang, *Phys. Rev. D* **64** (2001) 095003, [hep-ph/0105323](#); H. Abe, T. Kobayashi, N. Maru, and K. Yoshioka, *Phys. Rev. D* **67** (2003) 045019, [hep-ph/0205344](#); L. Randall, Y. Shadmi, and N. Weiner, *JHEP* **0301** (2003) 055, [hep-th/0208120](#); A. Katz and Y. Shadmi, *JHEP* **0411**, 060 (2004), [hep-th/0409223](#); C.D. Carone, J. Erlich, and B. Glover, *JHEP* **0510** (2005) 042, [hep-ph/0509002](#); J. de Blas, A. Falkowski, M. Perez-Victoria, and S. Pokorski, [hep-th/0605150](#).
- [17] M. Sremcević, R. Sazdanović, and S. Vukmirović,
<http://library.wolfram.com/infocenter/MathSource/4540>.

- [18] See, *e.g.*, G. 't Hooft and M.J.G. Veltman, *Annales Poincare Phys. Theor. A* **20** (1974) 69; M.J.G. Veltman, in *Les Houches 1975: Methods in Field Theory*, North-Holland, Amsterdam (1976); P. Van Nieuwenhuizen, *Phys. Rept.* **68** (1981) 189.
- [19] M. Fierz and W. Pauli, *Proc. Roy. Soc. Lond. A* **173** (1939) 211.
- [20] P. Creminelli, A. Nicolis, M. Papucci, and E. Trincherini, *JHEP* **0509**, 003 (2005), [hep-th/0505147](#).
- [21] F. Bauer, M. Lindner, and G. Seidl, *JHEP* **0405** (2004) 026, [hep-th/0309200](#).
- [22] T. Hällgren, T. Ohlsson, and G. Seidl, *JHEP* **0502** (2005) 049, [hep-ph/0411312](#).
- [23] H.D. Kim, *JHEP* **0601** (2006) 090, [hep-th/0510229](#).
- [24] See, *e.g.*, C.D. Hoyle, D.J. Kapner, B.R. Heckel, E.G. Adelberger, J.H. Gundlach, U. Schmidt, and H.E. Swanson, *Phys. Rev. D* **70** (2004) 042004, [hep-ph/0405262](#).
- [25] S. Hannestad and G.G. Raffelt, *Phys. Rev. Lett.* **88** (2001) 071301, [hep-ph/0110067](#).
- [26] L.J. Hall and D.R. Smith, *Phys. Rev. D* **60** (1999) 085008, [hep-ph/9904267](#); S. Hannestad, *Phys. Rev. D* **64** (2001) 023515, [hep-ph/0102290](#).
- [27] G.F. Giudice, R. Rattazzi, and J.D. Wells, *Nucl. Phys. B* **544** (1999), [hep-ph/9811291](#).
- [28] N. Arkani-Hamed, S. Dimopoulos, G.R. Dvali, and J. March-Russell, *Phys. Rev. D* **65** (2002) 024032, [hep-ph/9811448](#); K.R. Dienes, E. Dudas, and T. Gherghetta, *Nucl. Phys. B* **557** (1999) 25, [hep-ph/9811428](#); G.R. Dvali and A.Y. Smirnov, *Nucl. Phys. B* **563** (1999) 63, [hep-ph/9904211](#).
- [29] W. Skiba and D. Smith, *Phys. Rev. D* **65** (2002) 095002, [hep-ph/0201056](#)
- [30] See, *e.g.*, R. Barbieri, P. Creminelli and A. Strumia, *Nucl. Phys. B* **585** (2000) 28, [hep-ph/0002199](#), and references therein.
- [31] I. Kirsch, *Phys. Rev. D* **72** (2005) 024001, [hep-th/0503024](#); N. Boulanger and I. Kirsch, *Phys. Rev. D* **73** (2006) 124023, [hep-th/0602225](#).
- [32] F. Bauer and G. Seidl, *Phys. Lett. B* **624**, 250 (2005), [hep-ph/0506184](#); T. Hällgren and T. Ohlsson, *JCAP* **0606** (2006) 014, [hep-ph/0510174](#).